Eur. Phys. J. C 18, 681–709 (2001)
Digital Object Identifier (DOI) 10.1007/s100520100562

THE EUROPEAN PHYSICAL JOURNAL C

Charmless decays $B \to \mathrm{PP}, \mathrm{PV}$, and the effects of new strong and electroweak penguins in topcolor-assisted technicolor model

Z.J. Xiao[1,2,3], W.J. Li[2], L.B. Guo[1,4], G.R. Lu[1,2]

[1] CCAST(World Laboratory) P.O. Box 8730, Beijing 100080, P.R. China
[2] Department of Physics, Henan Normal University, Xinxiang 453002, P.R. China
[3] Department of Physics, Peking University, Beijing 100871, P.R. China
[4] Department of Physics, Wuhan University, Wuhan 430000, P.R. China

Received: 18 August 2000 / Revised version: 22 October 2000 /
Published online: 5 February 2001 – © Springer-Verlag 2001

Abstract. Based on the low energy effective Hamiltonian with generalized factorization, we calculate the new physics contributions to the branching ratios and CP-violating asymmetries of the two-body charmless hadronic decays $B \to \mathrm{PP}, \mathrm{PV}$ from the new strong and electroweak penguin diagrams in the topcolor-assisted technicolor (TC2) model. The top-pion penguins dominate the new physics corrections, and both new gluonic and electroweak penguins contribute effectively to most decay modes. For tree-dominated decay modes $B \to \pi\pi, \rho\pi$, etc. the new physics corrections are less than 10%. For decays $B \to K^{(*)}\pi$, $K^{(*)}\eta$, $\pi^0\eta^{(\prime)}$, $\eta^{(\prime)}\eta^{(\prime)}$, $K\overline{K}^0$, $\overline{K}^{*0}K$, etc. the new physics enhancements can be rather large (from -70% to $\sim 200\%$) and are insensitive to the variations of N_c^{eff}, k^2, η and $m_{\tilde{\pi}}$ within reasonable ranges. For the decays $B^0 \to \phi\pi$, $\phi\eta^{(\prime)}$, $K^*\overline{K}^0$ and ρ^+K^0, $\delta\mathcal{B}$ is strongly N_c^{eff} dependent: varying from -90% to $\sim 1680\%$ in the range of $N_c^{\mathrm{eff}} = 2$–∞. The new physics corrections to the CP-violating asymmetries $\mathcal{A}_{CP}$ vary greatly for different B decay channels. For five measured CP asymmetries of the $B \to K\pi, K\eta', \omega\pi$ decays, $\delta\mathcal{A}_{CP}$ is only about 20% and will be masked by large theoretical uncertainties. The new physics enhancements to interesting $B \to K\eta'$ decays are significant in size ($\sim 50\%$), insensitive to the variations of the input parameters and hence lead to a plausible interpretation for the unexpectedly large $B \to K\eta'$ decay rates. The TC2 model predictions for branching ratios and CP-violating asymmteries of all fifty-seven $B \to \mathrm{PP}, \mathrm{PV}$ decay modes are consistent with the available data within one or two standard deviations.

1 Introduction

The main goals of B experiments performed by CLEO, BarBar, Belle and other collaborations are to explore the physics of CP-violation, to test the standard model (SM) at an unexpected level of precision, and to perform an exhaustive search for possible effects of physics beyond the SM [1,2]. Precision measurements of the B meson system can provide insight into very high energy scales via the indirect loop effects of new physics (NP). The B system therefore offers a complementary probe to the search for new physics at the Tevatron, LHC and NLC, and in some cases may yield a constraint which surpasses those from direct searches or rules out some kinds of NP models [1].

In B experiments, new physics beyond the standard model may manifest itself, for example, in the following ways [1,3]:
(1) decays which are expected to be rare in the standard model are found to have large branching ratios;
(2) CP-violating asymmetries which are expected to vanish or be very small in the SM are found to be significantly large or with a very different pattern with what predicted in the SM;
(3) mixing in B decays is found to differ significantly from SM predictions.

These potential deviations may originate from the virtual effects of new physics through box and/or penguin diagrams in various new physics models [4–9].

Due to the anticipated importance of two-body charmless hadronic decays, $B \to h_1h_2$ (where h_1 and h_2 are the light pseudo-scalar (P) and/or vector (V) mesons), in understanding the phenomenon of CP-violation, a great effort have been made by many authors [10–14]. It is well known that the low energy effective Hamiltonian is the basic tool to calculate the branching ratios and A_{CP} of B meson decays. The short-distance QCD corrected Lagrangian at NLO level is available now, but we do not know how to calculate hadronic matrix elements from first principles. One conventionally resorts to the factorization approximation [15]. However, we also know that a non-factorizable contribution really exists and cannot be neglected numerically for most hadronic B decay channels. To remedy problems with the factorization hypothesis, some authors [16,12,13] introduced a phenomenological parameter N_{eff} (i.e. the effective number of colors) to model the non-factorizable contribution to the hadronic matrix element, which is commonly called the generalized factorization.

On the other hand, as pointed out by Buras and Silverstrini [17], such a generalization suffers from the problems of gauge and infrared dependence since the constant matrix $\hat{r}_{\mathrm{V}}$ appearing in the expressions of C_i^{eff} depends on both the gauge chosen and the external momenta. Very recently, Cheng et al. [18] studied and resolved the above controversies on the gauge dependence and infrared singularity of C_i^{eff} by using the perturbative QCD factorization theorem. Based on this progress, Chen et al. [14] calculated the charmless hadronic two-body decays of the B_u and B_d mesons within the framework of the generalized factorization, in which the effective Wilson coefficients C_i^{eff} are gauge invariant, infrared safe, and renormalization-scale and -scheme independent.

On the experimental side, the observation of thirteen $B \to \mathrm{PP}, \mathrm{PV}$ decays by CLEO, BaBar and Belle collaborations [19–25] signaled the beginning of the golden age of B physics. For $B \to K\pi, \pi\pi$ decays, the data are well accounted for in the effective Hamiltonian [27,28] with the generalized factorization approach [15,12,14]. For $B \to K\eta'$ decays, however, the unexpectedly large decay rate $\mathcal{B}(B \to K\eta') = (80^{+10}_{-9} \pm 7) \times 10^{-6}$ [20] still has no completely satisfactory explanation and has aroused considerable controversy [29].

In this paper, we will present our systematic calculation of branching ratios and CP-violating asymmetries for two-body charmless hadronic decays $B \to \mathrm{PP}$, PV (with charged B_u, neutral B_d mesons) in the framework of the topcolor-assisted technicolor (TC2) model [30] by employing the effective Hamiltonian with the generalized factorization. Since the scale of new strong interactions is expected to be around 1 TeV, the tree-level new physics contributions are strongly suppressed and will be neglected. We therefore will focus on the loop effects of new physics on two-body charmless hadronic B meson decays. We will evaluate analytically all new strong and electroweak penguin diagrams induced by exchanges of charged top-pions $\tilde{\pi}^{\pm}$ and technipions $\pi_1^{\pm}$ and $\pi_8^{\pm}$ in the quark level processes $b \to sV^*$ with $V = \gamma$, gluon, Z, and then combine the new physics contributions with their SM counterparts, find the effective Wilson coefficients and finally calculate the new physics contributions to the branching ratios and CP-violating asymmetries for all fifty-seven decay modes under consideration. We will concentrate on the new physics effects on charmless $B \to \mathrm{PP}, \mathrm{PV}$ decays and compare the theoretical predictions in the TC2 model with the SM predictions as well as the experimental measurements. For the phenomenologically interesting $B \to K\eta'$ decays, we found that the new physics enhancements are significant in size, $\sim 50\%$, insensitive to the variations of the input parameters and hence lead to a plausible interpretation for the large $B \to K\eta'$ decay rates.

This paper is organized as follows. In Sect. 2, we describe the basic structure of the TC2 model and examine the allowed parameter space of the TC2 model from currently available data. In Sect. 3, we give a brief review of the effective Hamiltonian, and then evaluate analytically the new penguin diagrams and find the effective Wilson coefficients C_i^{eff} and effective numbers a_i with the inclusion of new physics contributions. In Sects. 4 and 5, we calculate and show the numerical results of branching ratios and CP-violating asymmetries for all fifty-seven $B \to \mathrm{PP}, \mathrm{PV}$ decay modes, respectively. We concentrate on modes with a well-measured branching ratio and sizable yields. The conclusions and discussions are included in the final section.

2 TC2 model and experimental constraint

Apart from some differences in group structure and/or particle contents, all TC2 models [30,31] have the following common features:

(a) strong topcolor interactions, broken near 1 TeV, induce a large top condensate and all but a few GeV of the top quark mass, but contribute little to electroweak symmetry breaking;
(b) technicolor [32] interactions are responsible for electroweak symmetry breaking, and extended technicolor (ETC) [33] interactions generate the hard masses of all quarks and leptons, except those of the top quarks;
(c) there exist top-pions $\tilde{\pi}^{\pm}$ and $\tilde{\pi}^0$ with a decay constant $F_{\tilde{\pi}} \approx 50\,\mathrm{GeV}$. In this paper we will choose the well-motivated and most frequently studied TC2 model proposed by Hill [30] as the typical TC2 model to calculate the contributions to the charmless hadronic B decays in question from the relatively light unit-charged pseudoscalars. It is straightforward to extend the studies in this paper to other TC2 models.

In the TC2 model [30], after integrating out the heavy coloron and Z', the effective four-fermion interactions have the form [34]

$$\mathcal{L}_{\mathrm{eff}} = \frac{4\pi}{M_{\mathrm{V}}^2}\left\{ \left(\kappa + \frac{2\kappa_1}{27}\right)\overline{\psi}_{\mathrm{L}} t_{\mathrm{R}} \bar{t}_{\mathrm{R}} \psi_{\mathrm{L}} + \left(\kappa - \frac{\kappa_1}{27}\right)\overline{\psi}_{\mathrm{L}} b_{\mathrm{R}} \bar{b}_{\mathrm{R}} \psi_{\mathrm{L}} \right\}, \quad (1)$$

where $\kappa = (g_3^2/4\pi)\cot^2\theta$ and $\kappa_1 = (g_1^2/4\pi)\cot^2\theta'$, and M_{V} is the mass of the coloron V^{α} and Z'. The effective interactions of (1) can be written in terms of two auxiliary scalar doublets ϕ_1 and ϕ_2. Their couplings to the quarks are given by [35]

$$\mathcal{L}_{\mathrm{eff}} = \lambda_1 \overline{\psi}_{\mathrm{L}} \phi_1 \bar{t}_{\mathrm{R}} + \lambda_2 \overline{\psi}_{\mathrm{L}} \phi_2 \bar{b}_{\mathrm{R}}, \quad (2)$$

where $\lambda_1^2 = 4\pi(\kappa + 2\kappa_1/27)$ and $\lambda_2^2 = 4\pi(\kappa - \kappa_1/27)$. At energies below the topcolor scale $\Lambda \sim 1\,\mathrm{TeV}$ the auxiliary fields acquire kinetic terms, becoming physical degrees of freedom. The properly renormalized ϕ_1 and ϕ_2 doublets take the form

$$\phi_1 = \begin{pmatrix} F_{\tilde{\pi}} + \frac{1}{\sqrt{2}}(h_t + \mathrm{i}\tilde{\pi}^0) \\ \tilde{\pi}^- \end{pmatrix},$$

$$\phi_2 = \begin{pmatrix} \tilde{H}^+ \\ \frac{1}{\sqrt{2}}(\tilde{H}^0 + \mathrm{i}\tilde{A}^0) \end{pmatrix}, \quad (3)$$

where $\tilde{\pi}^\pm$ and $\tilde{\pi}^0$ are the top-pions, $\tilde{H}^{\pm,0}$ and $\tilde{A}^0$ are the b-pions, h_t is the top-Higgs, and $F_{\tilde{\pi}} \approx 50\,\mathrm{GeV}$ is the top-pion decay constant.

From (2), the couplings of top-pions to t- and b-quark can be written [30]

$$\frac{m_t^*}{F_{\tilde{\pi}}}\left[\mathrm{i}\bar{t}t\tilde{\pi}^0 + \mathrm{i}\bar{t}_\mathrm{R} b_\mathrm{L}\tilde{\pi}^+ + \mathrm{i}\frac{m_b^*}{m_t^*}\bar{t}_\mathrm{L} b_\mathrm{R}\tilde{\pi}^+ + \mathrm{h.c.}\right], \quad (4)$$

where $m_t^* = (1-\epsilon)m_t$ and $m_b^* \approx 1\,\mathrm{GeV}$ denote the masses of top and bottom quarks generated by the topcolor interactions.

For the mass of the top-pions, the current $1-\sigma$ lower mass bound from the Tevatron data is $m_{\tilde{\pi}} \geq 150\,\mathrm{GeV}$ [31], while the theoretical expectation is $m_{\tilde{\pi}} \approx (150\text{–}300\,\mathrm{GeV})$ [30]. For the mass of the b-pions, the current theoretical estimate is $m_{\tilde{H}^0} \approx m_{\tilde{A}^0} \approx (100\text{–}350)\,\mathrm{GeV}$ and $m_{\tilde{H}} = m_{\tilde{H}^0}^2 + 2m_t^2$ [36]. For the technipions $\pi_1^\pm$ and $\pi_8^\pm$, the theoretical estimates are $m_{\pi_1} \geq 50\,\mathrm{GeV}$ and $m_{\pi_8} \approx 200\,\mathrm{GeV}$ [37,38]. The effective Yukawa couplings of ordinary technipions $\pi_1^\pm$ and $\pi_8^\pm$ to fermion pairs, as well as the gauge couplings of unit-charged scalars to gauge bosons γ, Z^0 and gluon are basically model-independent; they can be found in [37–39].

At low energy, potentially large flavor-changing neutral currents (FCNC) arise when the quark fields are rotated from their weak eigenbasis to their mass eigenbasis, realized by the matrices $U_{\mathrm{L,R}}$ for the up-type quarks, and by $D_{\mathrm{L,R}}$ for the down-type quarks. When we make the replacements, for example,

$$b_\mathrm{L} \to D_\mathrm{L}^{bd} d_\mathrm{L} + D_\mathrm{L}^{bs} s_\mathrm{L} + D_\mathrm{L}^{bb} b_\mathrm{L}, \quad (5)$$

$$b_\mathrm{R} \to D_\mathrm{R}^{bd} d_\mathrm{R} + D_\mathrm{R}^{bs} s_\mathrm{R} + D_\mathrm{R}^{bb} b_\mathrm{R}, \quad (6)$$

the FCNC interactions will be induced. In the TC2 model, the corresponding flavor-changing effective Yukawa couplings are

$$\frac{m_t^*}{F_{\tilde{\pi}}}[\mathrm{i}\tilde{\pi}^+(D_\mathrm{L}^{bs}\bar{t}_\mathrm{R} s_\mathrm{L} + D_\mathrm{L}^{bd}\bar{t}_\mathrm{R} d_\mathrm{L}) + \mathrm{i}\tilde{H}^+(D_\mathrm{R}^{bs}\bar{t}_\mathrm{L} s_\mathrm{R} + D_\mathrm{R}^{bd}\bar{t}_\mathrm{L} d_\mathrm{R}) + \mathrm{h.c.}]. \quad (7)$$

For the mixing matrices in the TC2 model, authors usually use the "square-root ansatz": to take the square root of the standard model CKM matrix ($V_\mathrm{CKM} = U_\mathrm{L}^+ D_\mathrm{L}$) as an indication of the size of realistic mixings. It should be denoted that the square-root ansatz must be modified because of the strong constraint from the data of B^0–$\overline{B^0}$ mixing [35,40,41]. In TC2 model, the neutral scalars $\tilde{H}^0$ and $\tilde{A}^0$ can induce a contribution to the $B_q^0-\overline{B_q^0}$ $(q = d, s)$ mass difference [34,35]

$$\frac{\Delta M_{B_q}}{M_{B_q}} = \frac{7}{12}\frac{m_t^2}{F_{\tilde{\pi}}^2 m_{\tilde{H}^0}^2}\delta_{bq} B_{B_q} F_{B_q}^2, \quad (8)$$

where M_{B_q} is the mass of B_q meson, F_{B_q} is the B_q-meson decay constant, B_{B_q} is the renormalization group invariant parameter, and $\delta_{bq} \approx |D_\mathrm{L}^{bq} D_\mathrm{R}^{bq}|$. For the B_d meson, using the data of $\Delta M_{B_d} = (3.05 \pm 0.12) \times 10^{-10}\,\mathrm{MeV}$ [42] and setting $F_{\tilde{\pi}} = 50\,\mathrm{GeV}$, $B_{B_d}^{1/2} F_{B_d} = 200\,\mathrm{MeV}$, one has the bound $\delta_{bd} \leq 0.76 \times 10^{-7}$ for $m_{\tilde{H}^0} \leq 600\,\mathrm{GeV}$. This is an important and strong bound on the product of mixing elements $D_{\mathrm{L,R}}^{bd}$. As pointed out in [34], if one naively uses the square-root ansatz for *both* D_L and D_R, this bound is violated by about two orders of magnitudes. The constraint on both D_L and D_R from the data of the $b \to s\gamma$ decay is weaker than that from the B^0–$\bar{B}^0$ mixings [34]. By taking into account the above experimental constraints, we naturally can set $D_\mathrm{R}^{ij} = 0$ for $i \neq j$. Under this assumption, only the charged technipions $\pi_1^\pm, \pi_8^\pm$ and the charged top-pions $\tilde{\pi}^\pm$ contribute to the inclusive charmless decays $b \to s\bar{q}q, d\bar{q}q$ with $q \in \{u, d, s\}$ through the strong and electroweak penguin diagrams.

In the numerical calculations, we will use the "square-root ansatz" for D_L^{bd} and D_L^{bs}, i.e, setting $D_\mathrm{L}^{bd} = V_{td}/2$ and $D_\mathrm{L}^{bs} = V_{ts}/2$, respectively. We also fix the following parameters of the TC2 model in the numerical calculation[1]:

$$m_{\pi_1} = 100\,\mathrm{GeV}, \quad m_{\pi_8} = 200\,\mathrm{GeV}, \quad F_{\tilde{\pi}} = 50\,\mathrm{GeV}, \\ F_\pi = 120\,\mathrm{GeV}, \quad \epsilon = 0.05, \quad (9)$$

where F_π and $F_{\tilde{\pi}}$ are the decay constants for technipions and top-pions, respectively. For $m_{\tilde{\pi}}$, we consider the range of $m_{\tilde{\pi}} = 200 \pm 100\,\mathrm{GeV}$ to check the mass dependence of the branching ratios and CP-violating asymmetries of the charmless B decays.

3 Effective Hamiltonian and Wilson coefficients

We here present the well-known effective Hamiltonian for the two-body charmless decays $B \to h_1 h_2$. For more details on the effective Hamiltonian with generalized factorization for B decays, see for example [12,14,27,28].

3.1 Operators and Wilson coefficients in SM

The standard theoretical frame to calculate the inclusive three-body decays $b \to s\bar{q}q$[2] is based on the effective Hamiltonian [28,12]

$$\mathcal{H}_\mathrm{eff}(\Delta B = 1) = \frac{G_\mathrm{F}}{\sqrt{2}}\left\{\sum_{j=1}^{2} C_j (V_{ub}V_{us}^* Q_j^u + V_{cb}V_{cs}^* Q_j^c) - V_{tb}V_{ts}^*\left[\sum_{j=3}^{10} C_j Q_j + C_\mathrm{g} Q_\mathrm{g}\right]\right\}. \quad (10)$$

[1] From explicit numerical calculations in the next section, we know that the new physics contributions from the technipions $\pi_1^\pm$ and $\pi_8^\pm$ are much smaller than those from the top-pion $\tilde{\pi}^\pm$ within a reasonable parameter space. We therefore fix $m_{\pi_1} = 100\,\mathrm{GeV}$ and $m_{\pi_8} = 200\,\mathrm{GeV}$ for the sake of simplicity

[2] For $b \to d\bar{q}q$ decays, one simply makes the replacement $s \to d$

Here the operator basis reads

$$Q_1 = (\bar{s}q)_{V-A}(\bar{q}b)_{V-A},$$
$$Q_2 = (\bar{s}_\alpha q_\beta)_{V-A}(\bar{q}_\beta b_\alpha)_{V-A}, \tag{11}$$

with $q = u$ and $q = c$, and

$$Q_3 = (\bar{s}b)_{V-A} \sum_{q'} (\bar{q'}q')_{V-A},$$
$$Q_4 = (\bar{s}_\alpha b_\beta)_{V-A} \sum_{q'} (\bar{q'}_\beta q'_\alpha)_{V-A}, \tag{12}$$
$$Q_5 = (\bar{s}b)_{V-A} \sum_{q'} (\bar{q'}q')_{V+A},$$
$$Q_6 = (\bar{s}_\alpha b_\beta)_{V-A} \sum_{q'} (\bar{q'}_\beta q'_\alpha)_{V+A}, \tag{13}$$
$$Q_7 = \frac{3}{2}(\bar{s}b)_{V-A} \sum_{q'} e_{q'} (\bar{q'}q')_{V+A},$$
$$Q_8 = \frac{3}{2}(\bar{s}_\alpha b_\beta)_{V-A} \sum_{q'} e_{q'} (\bar{q'}_\beta q'_\alpha)_{V+A}, \tag{14}$$
$$Q_9 = \frac{3}{2}(\bar{s}b)_{V-A} \sum_{q'} e_{q'} (\bar{q'}q')_{V-A},$$
$$Q_{10} = \frac{3}{2}(\bar{s}_\alpha b_\beta)_{V-A} \sum_{q'} e_{q'} (\bar{q'}_\beta q'_\alpha)_{V-A}, \tag{15}$$
$$Q_{\mathrm{g}} = \frac{g_s}{8\pi^2} m_b \bar{s}_\alpha \sigma^{\mu\nu}(1+\gamma_5) T^a_{\alpha\beta} b_\beta G^a_{\mu\nu}, \tag{16}$$

where α and β are the $SU(3)$ color indices, and $T^a_{\alpha\beta}$ ($a = 1, ..., 8$) are the Gell-Mann matrices. The sum over q' runs over the quark fields that are active at the scale $\mu = O(m_b)$, i.e., $q' \in \{u, d, s, c, b\}$. The operator Q_1 and Q_2 are current–current operators, Q_3–Q_6 are QCD penguin operators induced by gluonic penguin diagrams, and the operators Q_7–Q_{10} are generated by electroweak penguins and box diagrams. The overall factor 2/3 is introduced for convenience, and the charge $e_{q'}$ is the charge of the quark q' with $q' = u, d, s, c, b$. The operator Q_{g} is the chromo-magnetic dipole operator generated from the magnetic gluon penguin. Following [12], we also neglect the effects of the electromagnetic penguin operator $Q_{7\gamma}$, and do not consider the effect of the weak annihilation and exchange diagrams.

Within the SM and at the scale M_W, the Wilson coefficients $C_1(M_W), \cdots, C_{10}(M_W)$ and $C_{\mathrm{g}}(M_W)$ have been given for example in [27,28]. They read in the naive dimensional regularization (NDR) scheme

$$C_1(M_W) = 1 - \frac{11}{6}\frac{\alpha_{\mathrm{s}}(M_W)}{4\pi} - \frac{35}{18}\frac{\alpha_{\mathrm{em}}}{4\pi},$$
$$C_2(M_W) = \frac{11}{2}\frac{\alpha_{\mathrm{s}}(M_W)}{4\pi},$$
$$C_3(M_W) = -\frac{\alpha_{\mathrm{s}}(M_W)}{24\pi}\left[E_0(x_t) - \frac{2}{3}\right] + \frac{\alpha_{\mathrm{em}}}{6\pi}\frac{1}{\sin^2\theta_W}[2B_0(x_t) + C_0(x_t)],$$
$$C_4(M_W) = \frac{\alpha_{\mathrm{s}}(M_W)}{8\pi}\left[E_0(x_t) - \frac{2}{3}\right],$$
$$C_5(M_W) = -\frac{\alpha_{\mathrm{s}}(M_W)}{24\pi}\left[E_0(x_t) - \frac{2}{3}\right],$$
$$C_6(M_W) = \frac{\alpha_{\mathrm{s}}(M_W)}{8\pi}\left[E_0(x_t) - \frac{2}{3}\right],$$
$$C_7(M_W) = \frac{\alpha_{\mathrm{em}}}{6\pi}\left[4C_0(x_t) + D_0(x_t) - \frac{4}{9}\right],$$
$$C_8(M_W) = 0,$$
$$C_9(M_W) = \frac{\alpha_{\mathrm{em}}}{6\pi}\left[4C_0(x_t) + D_0(x_t) - \frac{4}{9} + \frac{1}{\sin^2\theta_W}(10B_0(x_t) - 4C_0(x_t))\right],$$
$$C_{10}(M_W) = 0, \tag{17}$$
$$C_{\mathrm{g}}(M_W) = -\frac{E_0'(x_t)}{2}, \tag{18}$$

where $x_t = m_t^2/M_W^2$, the functions $B_0(x)$, $C_0(x)$, $D_0(x)$, $E_0(x)$ and $E_0'(x)$ are the familiar Inami–Lim functions [43],

$$B_0(x) = \frac{1}{4}\left[\frac{x}{1-x} + \frac{x\ln x}{(x-1)^2}\right], \tag{19}$$
$$C_0(x) = \frac{x}{8}\left[\frac{x-6}{x-1} + \frac{3x+2}{(x-1)^2}\ln x\right], \tag{20}$$
$$D_0(x) = -\frac{4}{9}\ln x + \frac{-19x^3 + 25x^2}{36(x-1)^3} + \frac{x^2(5x^2 - 2x - 6)}{18(x-1)^4}\ln x, \tag{21}$$
$$E_0(x) = \frac{18x - 11x^2 - x^3}{12(1-x)^3} - \frac{4 - 16x + 9x^2}{6(1-x)^4}\ln[x], \tag{22}$$
$$E_0'(x) = \left[\frac{2x + 5x^2 - x^3}{4(1-x)^3} + \frac{3x^2}{2(1-x)^4}\log[x]\right]. \tag{23}$$

Here the function $B_0(x)$ results from the evaluation of the box diagrams with leaving lepton pair $\nu\bar{\nu}$ or l^+l^- [28], the function $C_0(x)$ from the Z^0-penguin, the function $D_0(x)$ and $E_0(x)$ from the photon penguin and the gluon penguin diagram respectively, and finally the function $E_0'(x)$ arises from the magnetic gluon penguin.

By using QCD renormalization group equations [27, 28], it is straightforward to run Wilson coefficients $C_i(M_W)$ from the scale $\mu = 0(M_W)$ down to the lower scale $\mu = O(m_b)$. Working consistently to next-to-leading order (NLO) precision, the Wilson coefficients C_i for $i = 1, \ldots, 10$ are needed in NLO precision, while it is sufficient to use the leading logarithmic value for C_{g}. At the NLO level, the Wilson coefficients are usually renormalization-scheme (RS) dependent. In the NDR scheme, by using

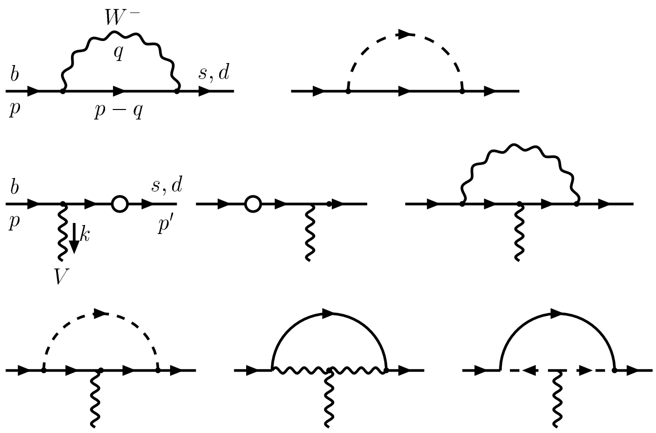

Fig. 1. Typical self-energy and penguin diagrams for the quark level decays $b \to (s,d)V^*$ ($V = \gamma, Z^0, g$), with $W^\pm$ (internal wave lines) and charged pseudo-scalar exchanges (internal dash lines) in the SM and TC2 model. The internal quarks are the upper type quark u, c and t

the input parameters as given in Appendix A and setting $\mu = 2.5\,\mathrm{GeV}$, we find

$$\begin{aligned} &C_1 = 1.1245, \quad C_2 = -0.2662, \quad C_3 = 0.0186, \\ &C_4 = -0.0458, \quad C_5 = 0.0113, \quad C_6 = -0.0587, \\ &C_7 = -5.5 \times 10^{-4}, \quad C_8 = 6.8 \times 10^{-4}, \\ &C_9 = -0.0095, \quad C_{10} = 0.0026, \quad C_g^{\mathrm{eff}} = -0.1527. \end{aligned} \tag{24}$$

Here, $C_g^{\mathrm{eff}} = C_{\mathrm{g}} + C_5$. These NLO Wilson coefficients are renormalization-scale and -scheme dependent, but such a dependence will be canceled by the corresponding dependence in the matrix elements of the operators in $\mathcal{H}_{\mathrm{eff}}$, as shown explicitly in [28,44].

3.2 New strong and electroweak penguins in the TC2 model

For the charmless hadronic decays of the B meson under consideration, the new physics will manifest itself by modifying the corresponding Inami–Lim functions $C_0(x)$, $D_0(x)$, $E_0(x)$ and $E_0'(x)$ which determine the coefficients $C_3(M_W), \ldots, C_{10}(M_W)$ and $C_{\mathrm{g}}(M_W)$, as illustrated in (17) and (18). These modifications, in turn, will change for example the standard model predictions for the branching ratios and CP-violating asymmetries for the decays $B \to h_1 h_2$.

The new strong and electroweak penguin diagrams can be obtained from the corresponding penguin diagrams in the SM by replacing the internal $W^\pm$ lines with the unit-charged scalar ($\pi_1^\pm, \pi_8^\pm$ and $\tilde{\pi}^\pm$) lines, as shown in Fig. 1. In the analytical calculations of those penguin diagrams, we will use dimensional regularization to regulate all the ultraviolet divergences in the virtual loop corrections and adopt the $\overline{\mathrm{MS}}$ renormalization scheme. It is easy to show that all ultraviolet divergences are canceled for each kind of charged scalar, respectively.

Following the same procedure as in [41,43], we calculate analytically the new Z^0-penguin diagrams induced by the exchanges of the charged scalars $\pi_1^\pm, \pi_8^\pm$ and $\tilde{\pi}^\pm$, and we find the new C_0 function which describes the NP contributions to the Wilson coefficients through the new Z^0-penguin diagrams,

$$\begin{aligned} C_0^{TC2} = \frac{1}{\sqrt{2} G_{\mathrm{F}} M_W^2} &\left[\frac{m_{\tilde{\pi}}^2}{4F_{\tilde{\pi}}^2} T_0(y_t) + \frac{m_{\pi_1}^2}{3F_\pi^2} T_0(z_t) \right. \\ &\left. + \frac{8 m_{\pi_8}^2}{3F_\pi^2} T_0(\xi_t) \right], \end{aligned} \tag{25}$$

with

$$T_0(x) = -\frac{x^2}{8(1-x)} - \frac{x^2}{8(1-x)^2} \log[x], \tag{26}$$

where $y_t = m_t^{*2}/m_{\tilde{\pi}}^2$ with $m_t^* = (1-\epsilon)m_t$, $z_t = (\epsilon m_t)^2/m_{\pi_1}^2$, $\xi_t = (\epsilon m_t)^2/m_{\pi_8}^2$.

By evaluating the new γ-penguin diagrams induced by the exchanges of three kinds of charged pseudo-scalar ($\tilde{\pi}^\pm, \pi_1^\pm, \pi_8^\pm$), we find that

$$\begin{aligned} D_0^{\mathrm{TC2}} = &\left\{ \frac{1}{4\sqrt{2} G_{\mathrm{F}} F_{\tilde{\pi}}^2} F_0(y_t) \right. \\ &\left. + \frac{1}{3\sqrt{2} G_{\mathrm{F}} F_\pi^2} [F_0(z_t) + 8F_0(\xi_t)] \right\}, \end{aligned} \tag{27}$$

with

$$\begin{aligned} F_0(x) = &\frac{47 - 79x + 38x^2}{108(1-x)^3} \\ &+ \frac{3 - 6x^2 + 4x^3}{18(1-x)^4} \log[x]. \end{aligned} \tag{28}$$

By evaluating the new gluon-penguin diagrams induced by the exchanges of three kinds of charged pseudo-scalar ($\tilde{\pi}^\pm, \pi_1^\pm, \pi_8^\pm$) as has been done in [8,9], we find that

$$\begin{aligned} E_0^{\mathrm{TC2}} = &\left\{ \frac{1}{4\sqrt{2} G_{\mathrm{F}} F_{\tilde{\pi}}^2} I_0(y_t) + \frac{1}{3\sqrt{2} G_{\mathrm{F}} F_\pi^2} [I_0(z_t) \right. \\ &\left. + 8I_0(\xi_t) + 9N_0(\xi_t)] \right\}, \end{aligned} \tag{29}$$

$$\begin{aligned} E_0'^{\mathrm{TC2}} = &\left\{ \frac{1}{8\sqrt{2} G_{\mathrm{F}} F_{\tilde{\pi}}^2} K_0(y_t) + \frac{1}{6\sqrt{2} G_{\mathrm{F}} F_\pi^2} [K_0(z_t) \right. \\ &\left. + 8K_0(\xi_t) + 9L_0(\xi_t)] \right\}, \end{aligned} \tag{30}$$

with

$$I_0(x) = \frac{7 - 29x + 16x^2}{36(1-x)^3} - \frac{3x^2 - 2x^3}{6(1-x)^4} \log[x], \tag{31}$$

$$K_0(x) = -\frac{5 - 19x + 20x^2}{6(1-x)^3} + \frac{x^2 - 2x^3}{(1-x)^4} \log[x], \tag{32}$$

$$L_0(x) = -\frac{4 - 5x - 5x^2}{6(1-x)^3} - \frac{x - 2x^2}{(1-x)^4} \log[x], \tag{33}$$

$$N_0(x) = \frac{11 - 7x + 2x^2}{36(1-x)^3} + \frac{1}{6(1-x)^4} \log[x]. \tag{34}$$

Using the input parameters as given in Appendix A and (9), and assuming $m_{\tilde{\pi}} = 200\,\mathrm{GeV}$, we find numerically that

$$\{C_0, D_0, E_0, E'_0\}^{\mathrm{TC2}}|_{\mu=M_W} = \{1.27, 0.27, 0.66, -1.58\} \tag{35}$$

if only the new contributions from top-pion penguins are included, while

$$\{C_0, D_0, E_0, E'_0\}^{\mathrm{TC2}}|_{\mu=M_W} = \{0.0002, 0.03, 0.04, -0.14\} \tag{36}$$

if only the new contributions from the technipion penguins are included. It is evident that it is the charged top-pion $\tilde{\pi}^{\pm}$ that strongly dominates the NP contributions, while the technipions play a minor rule only. We therefore fix the masses of $\pi_1^{\pm}$ and $\pi_8^{\pm}$ in the following numerical calculations.

Using the input parameters as given in Appendix A and (9) and assuming $m_{\tilde{\pi}} = 200\,\mathrm{GeV}$, we find that

$$\{C_0, D_0, E_0, E'_0\}^{\mathrm{SM}}|_{\mu=M_W} = \{0.81, -0.48, 0.27, 0.19\}, \tag{37}$$

$$\{C_0, D_0, E_0, E'_0\}^{\mathrm{TC2}}|_{\mu=M_W} = \{1.27, 0.30, 0.71, -1.72\}. \tag{38}$$

It is easy to see that the new physics parts of the functions under study are comparable in size to their SM counterparts. The SM predictions, consequently, may be changed significantly through interference. For the C_0 and E_0 functions, they will interfere constructively. For the D_0 and E'_0 functions, on the contrary, they will interfere destructively. One also should note that the magnitude of ${E'}_0^{\mathrm{TC2}}$ is much larger than its SM counterpart, and hence ${E'}_0^{\mathrm{TC2}}$ will dominate in the interference. We will combine the two parts of the corresponding functions to define the functions as follows:

$$\begin{aligned}
C_0(M_W) &= C_0(M_W)^{\mathrm{SM}} + C_0(M_W)^{\mathrm{TC2}},\\
D_0(M_W) &= D_0(M_W)^{\mathrm{SM}} + D_0(M_W)^{\mathrm{TC2}},\\
E_0(M_W) &= E_0(M_W)^{\mathrm{SM}} + E_0(M_W)^{\mathrm{TC2}},\\
E'_0(M_W) &= {E'}_0(M_W)^{\mathrm{SM}} + {E'}_0(M_W)^{\mathrm{TC2}},
\end{aligned} \tag{39}$$

where the functions $D_0(M_W)^{\mathrm{SM}}$, $E_0(M_W)^{\mathrm{SM}}$, $C_0(M_W)^{\mathrm{SM}}$ and $E'_0(M_W)^{\mathrm{SM}}$ have been given in (20), (21, (22) and (23), respectively, while the functions $C_0(M_W)^{\mathrm{TC2}}$, $D_0(M_W)^{\mathrm{TC2}}$, $E_0(M_W)^{\mathrm{TC2}}$ and $E'_0(M_W)^{\mathrm{TC2}}$ have also been defined in (25), (27), (29), and (30), respectively.

Since the heavy charged pseudo-scalars appearing in the TC2 model have been integrated out at the scale M_W, the QCD running of the Wilson coefficients $C_i(M_W)$ down to the scale $\mu = O(m_b)$ after including the NP contributions will be the same as in the SM. In the NDR scheme, by using the input parameters as given in Appendix A and (9), and setting $m_{\tilde{\pi}} = 200\,\mathrm{GeV}$ and $\mu = 2.5\,\mathrm{GeV}$, we find that

$$\begin{aligned}
&C_1 = 1.1245, \quad C_2 = -0.2662, \quad C_3 = 0.0195,\\
&C_4 = -0.0441, \quad C_5 = 0.0111, \quad C_6 = -0.0535,\\
&C_7 = 0.0026, \quad C_8 = 0.0018, \quad C_9 = -0.0175,\\
&C_{10} = 0.0049, \quad C_g^{\mathrm{eff}} = 0.3735,
\end{aligned} \tag{40}$$

where $C_g^{\mathrm{eff}} = C_{\mathrm{g}} + C_5$. By comparing the Wilson coefficients in (40) with those given in (24), we find that the $C_{1,2}$ remain unchanged, $C_{3,4,5,6}$ changed moderately, and $C_{7,8,9,10}$ and C_g^{eff} changed significantly because of the inclusion of new physics contributions.

3.3 Effective Wilson coefficients

Using the generalized factorization approach for nonleptonic B meson decays, the renormalization-scale and -scheme independent effective Wilson coefficients C_i^{eff} $(i = 1, \ldots, 10)$ have been obtained in [16,13,12] by adding to $C_i(\mu)$ the contributions from vertex-type quark matrix elements, denoted by the anomalous dimensional matrix γ_{V} and the constant matrix $\hat{r}_{\mathrm{V}}$ as given for example in [12]. Very recently, Cheng et al. [18] studied and resolved the so-called gauge and infrared problems [17] of the generalized factorization approach. They found that the gauge invariance is maintained under radiative corrections by working in the physical on-mass-shell scheme, while the infrared divergence in radiative corrections should be isolated using the dimensional regularization and the resultant infrared poles are absorbed into the universal meson wave functions [18].

In the NDR scheme and for $SU(3)_C$, the effective Wilson coefficients C_i^{eff} can be written as [12,14]

$$\begin{aligned}
C_1^{\mathrm{eff}} &= C_1 + \frac{\alpha_{\mathrm{s}}}{4\pi}\left(\hat{r}_{\mathrm{V}}^T + \gamma_{\mathrm{V}}^T \log\frac{m_b}{\mu}\right)_{1j} C_j,\\
C_2^{\mathrm{eff}} &= C_2 + \frac{\alpha_{\mathrm{s}}}{4\pi}\left(\hat{r}_{\mathrm{V}}^T + \gamma_{\mathrm{V}}^T \log\frac{m_b}{\mu}\right)_{2j} C_j,\\
C_3^{\mathrm{eff}} &= C_3 + \frac{\alpha_{\mathrm{s}}}{4\pi}\left(\hat{r}_{\mathrm{V}}^T + \gamma_{\mathrm{V}}^T \log\frac{m_b}{\mu}\right)_{3j} C_j\\
&\quad - \frac{1}{6}\frac{\alpha_{\mathrm{s}}}{4\pi}(C_t + C_p + C_g),\\
C_4^{\mathrm{eff}} &= C_4 + \frac{\alpha_{\mathrm{s}}}{4\pi}\left(\hat{r}_{\mathrm{V}}^T + \gamma_{\mathrm{V}}^T \log\frac{m_b}{\mu}\right)_{4j} C_j\\
&\quad + \frac{1}{2}\frac{\alpha_{\mathrm{s}}}{4\pi}(C_t + C_p + C_g),\\
C_5^{\mathrm{eff}} &= C_5 + \frac{\alpha_{\mathrm{s}}}{4\pi}\left(\hat{r}_{\mathrm{V}}^T + \gamma_{\mathrm{V}}^T \log\frac{m_b}{\mu}\right)_{5j} C_j\\
&\quad - \frac{1}{6}\frac{\alpha_{\mathrm{s}}}{4\pi}(C_t + C_p + C_g),\\
C_6^{\mathrm{eff}} &= C_6 + \frac{\alpha_{\mathrm{s}}}{4\pi}\left(\hat{r}_{\mathrm{V}}^T + \gamma_{\mathrm{V}}^T \log\frac{m_b}{\mu}\right)_{6j} C_j\\
&\quad + \frac{1}{2}\frac{\alpha_{\mathrm{s}}}{4\pi}(C_t + C_p + C_g),\\
C_7^{\mathrm{eff}} &= C_7 + \frac{\alpha_{\mathrm{s}}}{4\pi}\left(\hat{r}_{\mathrm{V}}^T + \gamma_{\mathrm{V}}^T \log\frac{m_b}{\mu}\right)_{7j} C_j + \frac{\alpha_{ew}}{8\pi} C_e,
\end{aligned}$$

$$
\begin{aligned}
C_8^{\mathrm{eff}} &= C_8 + \frac{\alpha_{\mathrm{s}}}{4\pi}\left(\hat{r}_{\mathrm{V}}^T + \gamma_{\mathrm{V}}^T \log\frac{m_b}{\mu}\right)_{8j} C_j, \\
C_9^{\mathrm{eff}} &= C_9 + \frac{\alpha_{\mathrm{s}}}{4\pi}\left(\hat{r}_{\mathrm{V}}^T + \gamma_{\mathrm{V}}^T \log\frac{m_b}{\mu}\right)_{9j} C_j + \frac{\alpha_{ew}}{8\pi} C_e, \\
C_{10}^{\mathrm{eff}} &= C_{10} + \frac{\alpha_{\mathrm{s}}}{4\pi}\left(\hat{r}_{\mathrm{V}}^T + \gamma_{\mathrm{V}}^T \log\frac{m_b}{\mu}\right)_{10j} C_j,
\end{aligned} \tag{41}
$$

where the matrices $\hat{r}_{\mathrm{V}}$ and γ_{V} contain the process independent contributions from the vertex diagrams. Like [14], we here include vertex corrections to C_7–C_{10}[3]. The anomalous dimension matrix γ_{V} has been given explicitly, for example, in (2.17) of [14]. Note that the correct value of the element $(\hat{r}_{\mathrm{NDR}})_{66}$ and $(\hat{r}_{\mathrm{NDR}})_{88}$ should be 17 instead of 1 as pointed out in [45]. $\hat{r}_{\mathrm{V}}$ in the NDR scheme takes the form

$$
\hat{r}_{\mathrm{V}}^{\mathrm{NDR}} = \begin{pmatrix}
3 & -9 & 0 & 0 & 0 & 0 & 0 & 0 & 0 & 0 \\
-9 & 3 & 0 & 0 & 0 & 0 & 0 & 0 & 0 & 0 \\
0 & 0 & 3 & -9 & 0 & 0 & 0 & 0 & 0 & 0 \\
0 & 0 & -9 & 3 & 0 & 0 & 0 & 0 & 0 & 0 \\
0 & 0 & 0 & 0 & -1 & 3 & 0 & 0 & 0 & 0 \\
0 & 0 & 0 & 0 & -3 & 17 & 0 & 0 & 0 & 0 \\
0 & 0 & 0 & 0 & 0 & 0 & -1 & 3 & 0 & 0 \\
0 & 0 & 0 & 0 & 0 & 0 & -3 & 17 & 0 & 0 \\
0 & 0 & 0 & 0 & 0 & 0 & 0 & 0 & 3 & -9 \\
0 & 0 & 0 & 0 & 0 & 0 & 0 & 0 & -9 & 3
\end{pmatrix}. \tag{42}
$$

The functions C_t, C_p, and C_g in (41) describe the contributions arising from the penguin diagrams of the current–current $Q_{1,2}$ and the QCD operators Q_3–Q_6, and the tree-level diagram of the magnetic dipole operator Q_{g}, respectively. We here also follow the procedure of [13] of including the contribution of the magnetic gluon penguin operator Q_g. The effective Wilson coefficients in (41) are now renormalization-scheme and -scale independent and do not suffer from gauge and infrared problems. The functions C_t, C_p, and C_g are given in the NDR scheme by [12, 14][4]

$$
C_t = \left[\frac{2}{3} + \frac{\lambda_u}{\lambda_t} G(m_u) + \frac{\lambda_c}{\lambda_t} G(m_c)\right] C_1, \tag{43}
$$

$$
\begin{aligned}
C_p &= \left[\frac{4}{3} - G(m_q) - G(m_b)\right] C_3 \\
&\quad + \sum_{i=u,d,s,c,b} \left[\frac{2}{3} - G(m_i)\right](C_4 + C_6),
\end{aligned} \tag{44}
$$

$$
C_e = \frac{8}{9}\left[\frac{2}{3} + \frac{\lambda_u}{\lambda_t} G(m_u) + \frac{\lambda_c}{\lambda_t} G(m_c)\right](C_1 + 3C_2), \tag{45}
$$

$$
C_g = -\frac{2m_b}{\sqrt{\langle k^2 \rangle}} C_{\mathrm{g}}^{\mathrm{eff}}, \tag{46}
$$

[3] Numerically, such corrections are negligibly small

[4] The constant term $2/3$ in front of $C_4 + C_6$ in C_p was missed in [12], but recovered firstly in [14]

with $\lambda_{q'} \equiv V_{q'b} V_{q'q}^*$. The function $G(m, k, \mu)$ is of the form [46]

$$
G(m, k, \mu) = \frac{10}{9} - \frac{2}{3} \ln\left[\frac{m^2}{\mu^2}\right] + \frac{2\mu^2}{3m^2} - \frac{2(1+2z)}{3z} g(z), \tag{47}
$$

where $z = k^2/(4m^2)$, and

$$
g(z) = \begin{cases}
\sqrt{\dfrac{1-z}{z}} \arctan\left[\dfrac{z}{1-z}\right], & z < 1, \\
\sqrt{\dfrac{1-z}{4z}} \left[\ln\left[\dfrac{\sqrt{z} + \sqrt{z-1}}{\sqrt{z} - \sqrt{z-1}}\right] - \mathrm{i}\pi\right], & z > 1,
\end{cases} \tag{48}
$$

where k^2 is the momentum squared transferred by the gluon, photon or Z to the $q'\overline{q'}$ pair in inclusive three-body decays $b \to qq'\overline{q'}$, and m is the mass of the internal up-type quark in the penguin diagrams. For $k^2 > 4m^2$, an imaginary part of $g(z)$ will appear because of the generation of a strong phase at the $\bar{u}u$ and $\bar{c}c$ threshold [46–48].

For the two-body exclusive B meson decays any information on k^2 is lost in the factorization assumption, and it is not clear what "relevant" k^2 should be taken in the numerical calculation. Based on simple estimates involving two-body kinematics [49] or the investigations in the first paper of [10], one usually uses the "physical" range for k^2 [49,48,44,12,14],

$$
\frac{m_b^2}{4} \lesssim k^2 \lesssim \frac{m_b^2}{2}. \tag{49}
$$

Following [12,14], we use $k^2 = m_b^2/2$ in the numerical calculation and will consider the k^2 dependence of branching ratios and CP-violating asymmetries of the charmless B meson decays. In fact, the branching ratios considered here are not sensitive to the value of k^2 within a reasonable range of k^2, but the CP-violating asymmetries are sensitive to the variation of k^2.

4 Branching ratios of $B \to \mathrm{PP}, \mathrm{PV}$ decays

In numerical calculations, we focus on the new physics effects on the branching ratios and CP-violating asymmetries for $B \to \mathrm{PP}, \mathrm{PV}$ decays. For the standard model part, we will follow the procedure of [12] and compare our SM results with those given in [12,14]. Two sets of form factors at the zero momentum transfer from the BSW model [15], as well as lattice QCD and light-cone QCD sum rules (LQQSR) will be used, respectively. Explicit values of these form factors can be found in [12] and have also been listed in Appendix B.

Following [12], the fifty-seven decay channels under study in this paper are also classified into five different classes (for more details about the classification, see [12]) as listed in the tables. The first three and last two classes are tree-dominated and penguin-dominated decays, respectively.

(1) Class-I: including four decay modes, $B^0 \to \pi^-\pi^+$, $\rho^\pm\pi^\mp$ and $B^0 \to \rho^- K^+$, the large and $N_c^{\rm eff}$ stable coefficient a_1 play the major role.
(2) Class-II: including ten decay modes, for example $B^0 \to \pi^0\pi^0$, and the relevant coefficient for these decays is a_2 which shows a strong $N_c^{\rm eff}$ dependence.
(3) Class-III: including nine decay modes involving the interference of class-I and class-II decays, such as the decays $B^+ \to \pi\eta'$.
(4) Class-IV: including twenty-two $B \to$ PP, PV decay modes such as $B \to K\eta^{(\prime)}$ decays. The amplitudes of these decays involve one (or more) of the dominant penguin coefficients $a_{4,6,9}$ with constructive interference among them. The class-IV decays are $N_c^{\rm eff}$ stable.
(5) Class-V: including twelve $B \to$ PP, PV decay modes, such as $B \to \pi^0\eta^{(\prime)}$ and $B \to \phi K$ decays. Since the amplitudes of these decays involve large and delicate cancelations due to interference between strong $N_c^{\rm eff}$ dependent coefficients $a_{3,5,7,10}$ and the dominant penguin coefficients $a_{4,6,9}$, these decays are generally not stable against $N_c^{\rm eff}$.

4.1 Decay amplitudes in the BSW model

With the factorization ansatz [15,12,14], the three-hadron matrix elements or the decay amplitude $\langle XY|H_{\rm eff}|B\rangle$ can be factorized into a sum of products of two current matrix elements, $\langle X|J_1^\mu|0\rangle$ and $\langle Y|J_{2\mu}|B\rangle$ (or $\langle Y|J_1^\mu|0\rangle$ and $\langle X|J_{2\mu}|B\rangle$). The former matrix elements are simply given by the corresponding decay constants f_X and g_X [50];

$$\langle 0|J_\mu|X(0^-)\rangle = {\rm i} f_X k_\mu, \langle 0|J_\mu|X(1^-)\rangle = M_X g_X \epsilon_\mu, \quad (50)$$

where f_X (g_X) is the decay constant of the pseudoscalar (vector) meson, and ϵ_μ is the polarization vector of the vector meson. For the second matrix element $\langle Y|J_{2\mu}|B\rangle$, the expression in terms of Lorentz-scalar form factors [15, 50] are of the form

$$\begin{aligned}
&\langle X(0^-)|J_\mu|B\rangle = \\
&\left[(k_B+k_X)_\mu - \frac{M_B^2-M_X^2}{k^2}k_\mu\right] F_1^{B\to X}(k^2) \\
&+\frac{M_B^2-M_X^2}{k^2}k_\mu F_0^{B\to X}(k^2), \quad (51)\\
&\langle X(1^-)|J_\mu|B\rangle = \\
&\frac{2}{M_B+M_X}\epsilon_{\mu\nu\rho\sigma}\epsilon^{*\nu}k_B^\rho k_X^\sigma V^{B\to X}(k^2) \\
&+{\rm i}\epsilon^*\cdot k\frac{2M_X}{k^2}k_\mu A_0(k^2) \\
&+{\rm i}(M_B+M_X)\left[\epsilon^*_\mu - \frac{\epsilon^*\cdot k}{k^2}k_\mu\right] A_1(k^2) \\
&-{\rm i}\frac{\epsilon^*\cdot k}{M_B+M_X} \\
&\times\left[(k_B+k_X)_\mu - \frac{M_B^2-M_X^2}{k^2}k_\mu\right] A_2(k^2), \quad (52)
\end{aligned}$$

where $k^\mu = k_B^\mu - k_X^\mu$ and M_B, M_X, M_Y are the masses of meson B, X and Y, respectively. The explicit expressions of form factors $F_{0,1}(k^2), V(k^2)$ and $A_{0,1,2}(k^2)$ have been given in Appendix B.

In the generalized factorization ansatz [12,14], the effective Wilson coefficients $C_i^{\rm eff}$ will appear in the decay amplitudes in the combinations

$$\begin{aligned}
a_{2i-1} &\equiv C_{2i-1}^{\rm eff} + \frac{C_{2i}^{\rm eff}}{N_c^{\rm eff}}, \\
a_{2i} &\equiv C_{2i}^{\rm eff} + \frac{C_{2i-1}^{\rm eff}}{N_c^{\rm eff}} \quad (i=1,\ldots,5), \quad (53)
\end{aligned}$$

where the effective number of colors $N_c^{\rm eff}$ is treated as a free parameter varying in the range of $2 \le N_c^{\rm eff} \le \infty$, in order to get a primary estimate of the size of the non-factorizable contribution to the hadronic matrix elements. It is evident that the reliability of the generalized factorization approach has been improved since the effective Wilson coefficients $C_i^{\rm eff}$ appearing in (53) are now gauge invariant and infrared safe. Although $N_c^{\rm eff}$ can in principle vary from channel to channel, in the energetic two-body hadronic B meson decays, it is expected to be process insensitive as supported by the data [14]. As argued in [16], $N_c^{\rm eff}$(LL) induced by the $(V-A)(V-A)$ operators can be rather different from $N_c^{\rm eff}$(LR) generated by $(V-A)(V+A)$ operators. Since we here focus on the calculation of new physics effects on the studied B meson decays induced by the new penguin diagrams in the TC2 model, we will simply assume that $N_c^{\rm eff}({\rm LL}) \equiv N_c^{\rm eff}({\rm LR}) = N_c^{\rm eff}$ and consider the variation of $N_c^{\rm eff}$ in the range of $2 \le N_c^{\rm eff} \le \infty$. For more details about the cases of $N_c^{\rm eff}({\rm LL}) \ne N_c^{\rm eff}({\rm LR})$, see for example [14]. We here will also not consider the possible effects of the final state interaction (FSI) and the contributions from annihilation channels, although they may play a significant rule for some $B \to$ PV, VV decays.

The effective coefficients a_i are displayed in Table 1 and Table 2 for the transitions $b \to d$ ($\bar b \to \bar d$) and $b \to s$ ($\bar b \to \bar s$), respectively. Theoretical predictions of a_i are made by using the input parameters as given in Appendix A and (9), and assuming $k^2 = m_b^2/2$ and $m_{\tilde\pi} = 200\,$GeV. For the coefficients $a_3, \ldots, a_{10}$, the first and second entries in Tables 1 and 2 refer to the values of a_i in the SM and TC2 model, respectively.

The new physics effects on the B decays under study will be included by using the modified effective coefficients a_i ($i=3,\ldots,10$) as given in the second entries of Tables 1 and 2. In the numerical calculations the input parameters as given in Appendix A, B and (9) will be used implicitly.

From Tables 1 and 2, one can find several interesting features of the coefficients a_i because of the inclusion of NP effects:

(a) the NP correction to the real part of the effective coefficients is around 20% for $a_{3,4,5,6}$, and can be as large as a factor of 4 for the coefficients $a_{7,8,9,10}$;
(b) the NP correction to the imaginary part of a_i is negligibly small;
(c) the coefficient a_1 and a_2 remain unchanged since we have neglected the very small tree-level NP contributions.

Table 1. Numerical values of a_i for the transitions $b \to d$ $[\bar{b} \to \bar{d}]$. The first and second entries for $a_3, \ldots, a_{10}$ refer to the values of a_i in the SM and TC2 model, respectively. The entries for $a_3, \ldots, a_{10}$ should be multiplied by 10^{-4}

	$N_c^{\mathrm{eff}} = 2$	$N_c^{\mathrm{eff}} = 3$	$N_c^{\mathrm{eff}} = \infty$
a_1	0.995 [0.995]	1.061 [1.061]	1.192 [1.192]
a_2	0.201 [0.201]	0.026 [0.026]	−0.395 [−0.395]
a_3	−16 − 7i [−25 − 23i]	77 [77]	261 + 13i [280 + 47i]
	−26 − 8i [−35 − 24i]	90 [90]	322 + 15i [340 + 49i]
a_4	−423 − 33i [−470 − 117i]	−467 − 35i [−517 − 125i]	−554 − 39i [−610 − 141i]
	−534 − 38i [−580 − 122i]	−588 − 40i [−638 − 130i]	−695 − 45i [−751 − 146i]
a_5	−192 − 7i [−202 − 23i]	−71 [−71]	171 + 13i [190 + 47i]
	−195 − 8i [−205 − 24i]	−57 [−57]	218 + 15i [237 + 49i]
a_6	−642 − 33i [−689 − 117i]	−671 − 35i [−721 − 125i]	−728 − 39i [−784 − 141i]
	−718 − 38i [−764 − 122i]	−754 − 40i [−804 − 130i]	−827 − 45i [−884 − 146i]
a_7	8.1 − 0.9i [7.7 − 1.7i]	6.9 − 0.9i [6.4 − 1.7i]	4.3 − 0.9i [3.9 − 1.7i]
	34 − 0.9i [34 − 1.7i]	31 − 0.9i [30 − 1.7i]	24.3 − 0.9i [23.9 − 1.7i]
a_8	9.7 − 0.5i [9.5 − 0.8i]	9.0 − 0.3i [8.8 − 0.6i]	7.5 [7.5]
	32 − 0.5i [31 − 0.8i]	28 − 0.3i [27 − 0.6i]	19.4 [19.4]
a_9	−83.7 − 0.9i [−84.1 − 1.7i]	−90 − 0.9i [−90 − 1.7i]	−102 − 0.9i [−102 − 1.7i]
	−153 − 0.9i [−153 − 1.7i]	−164 − 0.9i [−165 − 1.7i]	−187 − 0.9i [−188 − 1.7i]
a_{10}	−14.4 − 0.5i [−14.6 − 0.8i]	−2.6 − 0.3i [−2.5 − 0.6i]	37 [37]
	−25 − 0.5i [−25 − 0.8i]	−6.6 − 0.3i [−6.5 − 0.6i]	69 [69]

Table 2. Same as Table 1 but for the $b \to s$ $[\bar{b} \to \bar{s}]$ transitions

	$N_c^{\mathrm{eff}} = 2$	$N_c^{\mathrm{eff}} = 3$	$N_c^{\mathrm{eff}} = \infty$
a_1	0.995 [0.995]	1.061 [1.061]	1.192 [1.192]
a_2	0.201 [0.201]	0.026 [0.026]	−0.395 [−0.395]
a_3	−21 − 14i [−19 − 14i]	77 [77]	272 + 29i [269 + 29i]
	−31 − 15i [−30 − 15i]	90 [90]	332 + 31i [329 + 31i]
a_4	−449 − 72i [−442 − 72i]	−494 − 77i [−487 − 77i]	−585 − 86i [−576 − 86i]
	−560 − 77i [−553 − 77i]	−615 − 82i [−608 − 82i]	−725 − 92i [−717 − 92i]
a_5	−198 − 14i [−196 − 14i]	−71 [−71]	181 + 29i [179 + 29i]
	−200 − 15i [−199 − 15i]	−57 [−57]	229 + 31i [226 + 31i]
a_6	−667 − 72i [−661 − 72i]	−698 − 77i [−691 − 77i]	−758 − 86i [−750 − 86i]
	−744 − 77i [−737 − 77i]	−782 − 82i [−774 − 82i]	−858 − 92i [−850 − 92i]
a_7	7.9 − 1.3i [7.9 − 1.3i]	6.6 − 1.3i [6.7 − 1.3i]	4.1 − 1.3i [4.2 − 1.3i]
	34 − 1.3i [34 − 1.3i]	31 − 1.3i [31 − 1.3i]	24 − 1.3i [24 − 1.3i]
a_8	9.6 − 0.6i [9.6 − 0.6i]	8.9 − 0.4i [8.9 − 0.4i]	7.5 [7.5]
	32 − 0.6i [32 − 0.6i]	28 − 0.4i [28 − 0.4i]	19.4 [19.4]
a_9	−84 − 1.3i [−84 − 1.3i]	−90 − 1.3i [−90 − 1.3i]	−102 − 1.3i [−102 − 1.3i]
	−153 − 1.3i [−153 − 1.3i]	−165 − 1.3i [−164 − 1.3i]	−188 − 1.3i [−187 − 1.3i]
a_{10}	−14.5 − 0.6i [−14.5 − 0.6i]	−2.2 − 0.4i [−2.6 − 0.4i]	37 [37]
	−25 − 0.6i [−25 − 0.6i]	−6.6 − 0.4i [−6.6 − 0.4i]	69 [69]

4.2 Branching ratios of $B \to \mathrm{PP}$ decays

Using the above formulas, it is straightforward to find the decay amplitudes of $B \to \mathrm{PP}, \mathrm{PV}$. As an example, we present here the decay amplitude $M(B^- \to \pi^-\pi^0) = \langle \pi^-\pi^0 | H_{\mathrm{eff}} | B_u^- \rangle$,

$$\begin{aligned} M(B^- \to \pi^-\pi^0) &= \frac{G_\mathrm{F}}{2} \Big\{ V_{ub}V_{ud}^*(a_1 M_{uud}^{\pi^-\pi^0} + a_2 M_{duu}^{\pi^-\pi^0}) \\ &- V_{tb}V_{td}^* \Big[(a_4 + a_{10} + (a_6 + a_8)R_1) M_{duu}^{\pi^-\pi^0} \\ &- \Big(a_4 + \frac{3}{2}(a_7 - a_9) - \frac{a_{10}}{2} \\ &+ \Big(a_6 - \frac{a_8}{2} \Big) R_2 \Big) M_{uud}^{\pi^-\pi^0} \Big] \Big\}, \end{aligned} \tag{54}$$

with

$$R_1 = \frac{2m_{\pi^-}^2}{(m_b - m_u)(m_u + m_d)}, \tag{55}$$

$$R_2 = \frac{m_{\pi^0}^2}{m_d(m_b - m_d)}, \tag{56}$$

$$M_{uud}^{\pi^-\pi^0} = -\mathrm{i}(m_B^2 - m_{\pi^-}^2) f_\pi F_0^{B\pi}(m_{\pi^0}^2), \tag{57}$$

$$M_{duu}^{\pi^-\pi^0} = -\mathrm{i}(m_B^2 - m_{\pi^0}^2) f_\pi F_0^{B\pi}(m_{\pi^-}^2), \tag{58}$$

where f_π is the decay constant of the π meson. The form factor $F_0^{B\pi}(m^2)$ can be found in Appendix B. Under the approximation of setting $m_u = m_d$ and $m_{\pi^0} = m_{\pi^-}$, the decay amplitude $M(B^- \to \pi^-\pi^0)$ in (54) will be reduced to the same form as the one given in (80) of [12]:

$$\begin{aligned} M(B^- \to \pi^-\pi^0) &= -\mathrm{i}\frac{G_\mathrm{F}}{2} f_\pi F_0^{B\pi}(m_\pi^2)(m_B^2 - m_\pi^2) \\ &\times \Big\{ V_{ub}V_{ud}^*(a_1 + a_2) \\ &- V_{tb}V_{td}^* \frac{3}{2}(-a_7 + a_9 + a_{10} + a_8 R_2) \Big\}. \end{aligned} \tag{59}$$

In the following numerical calculations, we use the decay amplitudes as given in Appendix A of [12] directly without further discussions about the details.

In the B rest frame, the branching ratios of the two-body B meson decays can be written as

$$\mathcal{B}(B \to XY) = \frac{1}{\Gamma_{\mathrm{tot}}} \frac{|p|}{8\pi M_B^2} |M(B \to XY)|^2 \tag{60}$$

for the $B \to PP$ decays, and

$$\mathcal{B}(B \to XY) = \frac{1}{\Gamma_{\mathrm{tot}}} \frac{|p|^3}{8\pi M_\mathrm{V}^2} |M(B \to XY)/(\epsilon \cdot p_B)|^2 \tag{61}$$

for the $B \to \mathrm{PV}$ decays. Here $\Gamma_{\mathrm{tot}}(B_u^-) = 3.989 \times 10^{-13}\,\mathrm{GeV}$ and $\Gamma_{\mathrm{tot}}(B_d^0) = 4.219 \times 10^{-13}\,\mathrm{GeV}$; this is obtained by using $\tau(B_u^-) = 1.65\,\mathrm{ps}$ and $\tau(B_d^0) = 1.56\,\mathrm{ps}$ [42]. p_B is the four-momentum of the B meson, M_V and ϵ is the mass and polarization vector of the produced light vector meson respectively, and

$$|p| = \frac{1}{2M_B}\sqrt{[M_B^2 - (M_X + M_Y)^2][M_B^2 - (M_X - M_Y)^2]} \tag{62}$$

is the magnitude of the momentum of particle X and Y in the B rest frame.

In Tables 3–8, we present the numerical results of the branching ratios for the twenty $B \to \mathrm{PP}$ decays and thirty-seven $B \to \mathrm{PV}$ decays in the framework of the SM and TC2 model. The theoretical predictions are made by using the central values of the input parameters as given in (9) and Appendix A and B, and assuming $m_{\tilde{\pi}} = 200\,\mathrm{GeV}$ and $N_c^{\mathrm{eff}} = 2, 3, \infty$ in the generalized factorization approach. The k^2 dependence of the branching ratios is weak in the range of $k^2 = m_b^2/2 \pm 2\,\mathrm{GeV}^2$ and hence the numerical results are given by fixing $k^2 = m_b^2/2$. The currently available CLEO data [19–21] are listed in the last column. The branching ratios collected in the tables are the averages of the branching ratios of B and anti-B decays. The ratio $\delta\mathcal{B}$ describes the new physics corrections on the SM predictions of the corresponding branching ratios and is defined by

$$\delta\mathcal{B}(B \to XY) = \frac{\mathcal{B}(B \to XY)^{\mathrm{TC2}} - \mathcal{B}(B \to XY)^{\mathrm{SM}}}{\mathcal{B}(B \to XY)^{\mathrm{SM}}}. \tag{63}$$

By comparing the numerical results with the CLEO data, the following general features of $B \to \mathrm{PP}$ decays can be understood:

(1) The SM predictions for five measured $B^0 \to \pi^+\pi^-$ and $B \to K\pi$ decay modes are consistent with the CLEO data. But for the measured $B \to K\eta'$ decays, the observed branching ratios are clearly much larger than the SM predictions [11,12,14]. All other estimated branching ratios in Tables 3 and 4 are consistent with the new CLEO upper limits.
(2) The uncertainties of the SM predictions for the branching ratios of $B \to \mathrm{PP}$ decays induced by varying k^2 is $\sim 10\%$ within the range of $k^2 = m_b^2/2 \pm 2\,\mathrm{GeV}^2$.
(3) For most class-II, IV and V decay channels, such as $B \to \eta\eta^{(\prime)}$, $B \to K\pi$, $B \to K\eta'$, etc. the NP enhancements to the decay rates can be rather large: from 20% to 70% of the SM predictions.
(4) For most $B \to \mathrm{PP}$ decay channels, the magnitude of the NP effects is insensitive to the variations of $m_{\tilde{\pi}}$ and N_c^{eff}.
(5) The central values of the branching ratios obtained by using the LQQSR form factors will generally be increased by about 15% when compared with the results using the BSW form factors, as can be seen from Tables 3 and 4. Irrespective of whether the BSW or the LQQSR form factors were used, the magnitude and whole pattern of the new physics corrections to the decay rates of our study remain basically unchanged.
(6) Both new gluonic and electroweak penguin diagrams contribute effectively to most decay modes.

4.2.1 $B \to \pi\pi, K\pi$ decays

There are so far seven measured $B \to \mathrm{PP}$ decay modes [20,21,24,25]:

$$\mathcal{B}(B \to \pi^+\pi^-)$$

Table 3. $B \to$ PP branching ratios (in units of 10^{-6}) using the BSW form factors, with $k^2 = m_b^2/2$, $A = 0.81$, $\lambda = 0.2205$, $\rho = 0.12$, $\eta = 0.34$, $N_c^{\rm eff} = 2, 3, \infty$ and assuming $m_{\tilde{\pi}} = 200\,\mathrm{GeV}$, in the SM and TC2 model by employing generalized factorization approach. The last column contains the measured branching ratios and upper limits (90% C.L.) [19,20]

		SM			TC2			$\delta\mathcal{B}$[%]			
Channel	Class	2	3	∞	2	3	∞	2	3	∞	Data
$B^0 \to \pi^+\pi^-$	I	9.10	10.3	13.0	9.27	10.5	13.2	1.9	1.8	1.6	$4.3^{+1.6}_{-1.5} \pm 0.5$
$B^0 \to \pi^0\pi^0$	II	0.28	0.15	0.92	0.28	0.16	0.94	1.0	6.3	2.8	< 9.3
$B^+ \to \pi^+\pi^0$	III	6.41	5.06	2.85	6.41	5.07	2.85	0.1	0.1	0.1	< 12.7
$B^0 \to \eta\eta$	II	0.14	0.10	0.29	0.20	0.17	0.38	40	64	30	< 18
$B^0 \to \eta\eta'$	II	0.14	0.08	0.38	0.19	0.13	0.45	30	67	19	< 27
$B^0 \to \eta'\eta'$	II	0.05	0.01	0.13	0.04	0.02	0.14	13	73	7.8	< 47
$B^+ \to \pi^+\eta$	III	3.51	2.78	1.75	3.85	3.17	2.25	10	14	28	< 5.7
$B^+ \to \pi^+\eta'$	III	2.49	1.88	1.02	2.59	1.99	1.16	3.8	5.8	13	< 12
$B^0 \to \pi^0\eta$	V	0.26	0.29	0.39	0.36	0.42	0.57	42	44	46	< 2.9
$B^0 \to \pi^0\eta'$	V	0.06	0.08	0.14	0.08	0.10	0.18	37	35	26	< 5.7
$B^+ \to K^+\pi^0$	IV	12.0	13.5	16.7	19.6	21.8	26.5	63	61	59	$11.6^{+3.0+1.4}_{-2.7-1.3}$
$B^0 \to K^+\pi^-$	IV	17.8	19.8	24.0	24.4	26.9	32.2	37	36	35	$17.2^{+2.5}_{-2.4} \pm 1.2$
$B^+ \to K^0\pi^+$	IV	19.9	23.2	30.6	27.7	32.7	44.0	39	41	44	$18.2^{+4.6}_{-4.0} \pm 1.6$
$B^0 \to K^0\pi^0$	IV	7.27	8.31	10.7	7.95	9.36	12.6	9.3	13	18	$14.6^{+5.9+2.4}_{-5.1-3.3}$
$B^+ \to K^+\eta$	IV	3.91	4.56	6.07	4.09	5.08	7.45	4.6	11	23	< 6.9
$B^+ \to K^+\eta'$	IV	22.6	28.5	42.4	33.8	41.6	59.5	50	46	40	$80^{+10}_{-9} \pm 7$
$B^0 \to K^0\eta$	IV	3.22	3.63	4.58	3.33	3.90	5.23	3.6	7.5	14	< 9.3
$B^0 \to K^0\eta'$	IV	21.9	28.2	43.0	32.9	41.3	61.2	50	47	43	$89^{+18}_{-16} \pm 9$
$B^+ \to K^+\bar{K}^0$	IV	1.16	1.35	1.78	1.61	1.90	2.55	38	40	43	< 5.1
$B^0 \to K^0\bar{K}^0$	IV	1.10	1.28	1.68	1.52	1.80	2.41	38	40	43	< 17

$$= \begin{cases} (4.3^{+1.6}_{-1.5} \pm 0.5) \times 10^{-6} & [\text{CLEO}], \\ (9.3^{+2.8+1.2}_{-2.1-1.4}) \times 10^{-6} & [\text{BaBar}], \end{cases} \tag{64}$$

$$\mathcal{B}(B \to K^+\pi^0) = \begin{cases} (11.6^{+3.0+1.4}_{-2.7-1.3}) \times 10^{-6} & [\text{CLEO}], \\ (18.8^{+5.5}_{-4.9} \pm 2.3) \times 10^{-6} & [\text{Belle}], \end{cases} \tag{65}$$

$$\mathcal{B}(B \to K^+\pi^-) = \begin{cases} (17.2^{+2.5}_{-2.4} \pm 1.2) \times 10^{-6} & [\text{CLEO}], \\ (12.5^{+3.0+1.3}_{-2.6-1.7} \pm 2.3) \times 10^{-6} & [\text{BaBar}], \\ (17.4^{+5.1}_{-4.6} \pm 3.4) \times 10^{-6} & [\text{Belle}], \end{cases} \tag{66}$$

$$\mathcal{B}(B \to K^0\pi^+) = (18.2^{+4.6}_{-4.0} \pm 1.6) \times 10^{-6} \quad [\text{CLEO}], \tag{67}$$

$$\mathcal{B}(B \to K^0\pi^0) = \begin{cases} (14.6^{+5.9+2.4}_{-5.1-3.3}) \times 10^{-6} & [\text{CLEO}], \\ (21^{+9.3+2.5}_{-7.8-2.3}) \times 10^{-6} & [\text{Belle}], \end{cases} \tag{68}$$

$$\mathcal{B}(B \to K^+\eta') = \begin{cases} (80^{+10}_{-9} \pm 7) \times 10^{-6} & [\text{CLEO}], \\ (62 \pm 18 \pm 8) \times 10^{-6} & [\text{BaBar}], \end{cases} \tag{69}$$

$$\mathcal{B}(B \to K^0\eta') = (89^{+18}_{-16} \pm 9) \times 10^{-6} \quad [\text{CLEO}]. \tag{70}$$

The measurements of CLEO, BaBar and Belle are in good agreement within the errors.

Being in a class-I decay channel, the $B^0 \to \pi^+\pi^-$ decays are dominated by the $b \to u$ tree diagram. This mode together with the $B^0 \to \pi^0\pi^0$ and $B^+ \to \pi^+\pi^0$ decays play an important role in the determination of the angle α. For all three $B \to \pi\pi$ decay modes, the new penguin enhancement is very small, $\leq 6.3\%$ for $N_c^{\rm eff} = 2 - \infty$, as listed in Tables 3 and 4. The theoretical predictions in the SM and TC2 model are consistent with the CLEO data.

For $B^0 \to \eta^{(\prime)}\eta^{(\prime)}$ decays, the NP enhancement is varying in the range of 10% to 70%. For the $B^+ \to \pi^+\eta^{(\prime)}$ decays, the NP enhancement is around 10% and depends on $N_c^{\rm eff}$ moderately. For the $B^0 \to \pi^0\eta^{(\prime)}$ decays, the NP enhancement is large, 30%–60%, and insensitive to the variation of $N_c^{\rm eff}$.

In the SM, the four class-IV decays $B \to K\pi$ are dominated by the $b \to sg$ gluonic penguin diagram, with additional contributions from the $b \to u$ tree and electroweak penguin diagrams. Measurements of $B \to K\pi$ decays are particularly important for measuring the angle γ. In the TC2 model, the new penguin diagrams will interfere with their SM counterparts and change the SM predictions for the branching ratios and CP-violating asymmetries.

Table 4. Same as Table 3, but using the LQQSR form factors

		SM			TC2			$\delta\mathcal{B}[\%]$			
Channel	Class	2	3	∞	2	3	∞	2	3	∞	Data
$B^0 \to \pi^+\pi^-$	I	10.8	12.3	15.5	11.0	12.5	15.8	1.9	1.8	1.6	$4.3^{+1.6}_{-1.5} \pm 0.5$
$B^0 \to \pi^0\pi^0$	II	0.33	0.18	1.09	0.33	0.19	1.12	1.0	6.3	2.8	< 9.3
$B^+ \to \pi^+\pi^0$	III	7.62	6.02	3.39	7.63	6.03	3.39	0.1	0.1	0.1	< 12.7
$B^0 \to \eta\eta$	II	0.17	0.13	0.36	0.24	0.21	0.47	40	64	30	< 18
$B^0 \to \eta\eta'$	II	0.17	0.09	0.45	0.22	0.15	0.53	30	67	19	< 27
$B^0 \to \eta'\eta'$	II	0.05	0.01	0.15	0.05	0.02	0.16	13	73	7.8	< 47
$B^+ \to \pi^+\eta$	III	4.25	3.37	2.13	4.66	3.83	2.73	9.6	14	28	< 5.7
$B^+ \to \pi^+\eta'$	III	2.90	2.17	1.17	3.01	2.30	1.33	3.8	5.8	14	< 12
$B^0 \to \pi^0\eta$	V	0.31	0.35	0.47	0.43	0.50	0.69	42	44	46	< 2.9
$B^0 \to \pi^0\eta'$	V	0.07	0.09	0.17	0.09	0.12	0.21	37	36	26	< 5.7
$B^+ \to K^+\pi^0$	IV	14.3	16.0	19.8	23.2	25.8	31.4	63	61	58	$11.6^{+3.0+1.4}_{-2.7-1.3}$
$B^0 \to K^+\pi^-$	IV	21.2	23.5	28.5	29.0	32.0	38.4	37	36	35	$17.2^{+2.5}_{-2.4} \pm 1.2$
$B^+ \to K^0\pi^+$	IV	23.7	27.7	36.4	33.0	38.9	52.3	39	41	43	$18.2^{+4.6}_{-4.0} \pm 1.6$
$B^0 \to K^0\pi^0$	IV	8.68	9.92	12.7	9.51	11.2	15.1	9.6	13	18	$14.6^{+5.9+2.4}_{-5.1-3.3}$
$B^+ \to K^+\eta$	IV	4.37	5.10	6.80	4.54	5.66	8.33	3.9	11	22	< 6.9
$B^+ \to K^+\eta'$	IV	26.2	33.1	49.2	39.2	48.2	69.1	50	46	40	$80^{+10}_{-9} \pm 7$
$B^0 \to K^0\eta$	IV	3.57	4.02	5.07	3.67	4.30	5.76	2.8	6.8	14	< 9.3
$B^0 \to K^0\eta'$	IV	25.5	32.7	49.9	38.1	48.0	71.1	50	47	43	$89^{+18}_{-16} \pm 9$
$B^+ \to K^+\bar{K}^0$	IV	1.35	1.58	2.07	1.87	2.21	2.96	38	40	43	< 5.1
$B^0 \to K^0\bar{K}^0$	IV	1.28	1.49	1.96	1.77	2.09	2.80	38	40	43	< 17

It is well known that the effective Hamiltonian calculations of charmless hadronic B meson decays contain many uncertainties, including form factors, light quark masses, CKM matrix elements, the QCD scale and the external momentum k^2. As a simple illustration of the theoretical uncertainties, we calculate and show the branching ratios of four $B \to K\pi$ decay modes by using $F_0^{B\pi}(0) = 0.20$ (preferred by the CLEO measurement of $B \to \pi^+\pi^-$ mode [51]) instead of the ordinary BSW value $F_0^{B\pi}(0) = 0.33$ (all other input parameters remain unchanged) and by varying η, k^2 and $m_{\tilde{\pi}}$ in the ranges of $\eta = 0.34 \pm 0.08$, $k^2 = m_b^2/2 \pm 2\,\mathrm{GeV}^2$, $m_{\tilde{\pi}} = 200 \pm 100\,\mathrm{GeV}$, and setting $N_c^{\mathrm{eff}} = 2, 3, \infty$:

$$\mathcal{B}(B \to K^+\pi^0) = \begin{cases} (5.8 \pm 0.1^{+1.6+1.4}_{-0.4-0.7}) \times 10^{-6} \\ \quad \text{in SM}, \\ (10.1 \pm 0.1^{+1.0+2.3+2.2}_{-0.6-1.0-1.2}) \times 10^{-6} \\ \quad \text{in TC2}, \end{cases} \tag{71}$$

$$\mathcal{B}(B \to K^+\pi^-) = \begin{cases} (7.3 \pm 0.1^{+0.7+1.5}_{-0.5-0.8}) \times 10^{-6} \\ \quad \text{in SM}, \\ (9.9 \pm 0.1^{+1.2+1.90.7}_{-0.9-0.9-0.6}) \times 10^{-6} \\ \quad \text{in TC2}, \end{cases} \tag{72}$$

$$\mathcal{B}(B \to K^0\pi^+) = \begin{cases} (8.5 \pm 0.0^{+0.8+2.7}_{-1.5-1.2}) \times 10^{-6} \\ \quad \text{in SM}, \\ (12.0 \pm 0.0^{+1.5+4.2+1.2}_{-1.0-1.8-0.8}) \times 10^{-6} \\ \quad \text{in TC2}, \end{cases} \tag{73}$$

$$\mathcal{B}(B \to K^0\pi^0) = \begin{cases} (2.5 \pm 0.0^{+0.3+0.6}_{-0.2-0.3}) \times 10^{-6} \\ \quad \text{in SM}, \\ (2.3 \pm 0.0^{+0.4+0.8+0.1}_{-0.3-0.3-0.4}) \times 10^{-6} \\ \quad \text{in TC2}, \end{cases} \tag{74}$$

where the first, second and third error correspond to the uncertainty $\delta\eta = \pm 0.08$, $\delta q^2 = \pm 2$ and $2 \leq N_c^{\mathrm{eff}} \leq \infty$ respectively, while the fourth error refers to $\delta m_{\tilde{\pi}} = \pm 100\,\mathrm{GeV}$. By comparing the ratios in Tables 3, 4 and in (71)–(74), it is easy to see that the central values of the branching ratios $\mathcal{B}(B \to K\pi)$ are greatly reduced by using $F_0^{B\pi}(0) = 0.20$ instead of 0.33; the new physics enhancements therefore become essential to make the theoretical predictions consistent with the data.

Figure 2 shows the mass and N_c^{eff} dependence of the ratios $\mathcal{B}(B \to K^+\pi^0)$ in the SM and TC2 model using the input parameters as given in Appendix A and B and employing the BSW form factors. In Fig. 2a, we set $N_c^{\mathrm{eff}} = 2$ and assume that $m_{\tilde{\pi}} = 100$–$300\,\mathrm{GeV}$. In Fig. 2b, we set $m_{\tilde{\pi}} = 200\,\mathrm{GeV}$ and assume that $\xi = 1/N_c^{\mathrm{eff}} = 0 - 0.5$. In Fig. 2 the short-dashed line and solid curve show the branching ratio of $B^0 \to K^+\pi^0$ decay in the SM and TC2 model, respectively. The band between the two dotted lines corresponds to the CLEO data with 2σ errors: $\mathcal{B}(B \to K^+\pi^0) = (11.6^{+6.6}_{-6.0}) \times 10^{-6}$.

In the same way as in Fig. 2, Figs. 3, 4 and 5 show the mass and N_c^{eff} dependence of the branching ratios of the decay $B \to K^+\pi^0, K^+\pi^-, K^0\pi^+$ and $K^0\pi^0$, respectively. In these three figures, the short-dashed lines and

Table 5. Same as Table 3, but for branching ratios of $B \to \mathrm{PP}$ decays with new physics contributions from charged-scalar gluonic penguins only

		TC2: QCD only			$\delta\mathcal{B}[\%]$			
Channel	Class	2	3	∞	2	3	∞	Data
$B^0 \to \pi^+\pi^-$	I	9.27	10.5	13.3	1.90	1.86	1.90	$4.3^{+1.6}_{-1.5} \pm 0.5$
$B^0 \to \pi^0\pi^0$	II	0.34	0.22	1.01	23.3	47.9	9.85	< 9.3
$B^+ \to \pi^+\pi^0$	III	6.41	5.06	2.85	0.0	0.0	0.0	< 12.7
$B^0 \to \eta\eta$	II	0.17	0.14	0.34	23.8	37.1	16.5	< 18
$B^0 \to \eta\eta'$	II	0.19	0.13	0.45	32.1	68.7	17.7	< 27
$B^0 \to \eta'\eta'$	II	0.05	0.02	0.15	29.3	162	16.9	< 47
$B^+ \to \pi^+\eta$	III	3.75	3.05	2.10	6.86	9.86	19.7	< 5.7
$B^+ \to \pi^+\eta'$	III	2.65	2.05	1.25	6.11	9.38	21.8	< 12
$B^0 \to \pi^0\eta$	V	0.36	0.41	0.54	40.2	40.5	37.8	< 2.9
$B^0 \to \pi^0\eta'$	V	0.12	0.15	0.24	107	97.2	65.2	< 5.7
$B^+ \to K^+\pi^0$	IV	16.0	18.0	22.4	33.0	33.5	34.1	$11.6^{+3.0+1.4}_{-2.7-1.3}$
$B^0 \to K^+\pi^-$	IV	24.5	27.3	33.3	37.7	38.2	39.1	$17.2^{+2.5}_{-2.4} \pm 1.2$
$B^+ \to K^0\pi^+$	IV	27.3	31.7	41.5	37.0	36.5	35.7	$18.2^{+4.6}_{-4.0} \pm 1.6$
$B^0 \to K^0\pi^0$	IV	10.4	11.8	15.1	42.5	42.4	42.0	$14.6^{+5.9+2.4}_{-5.1-3.3}$
$B^+ \to K^+\eta$	IV	5.02	5.90	7.95	28.4	29.4	30.8	< 6.9
$B^+ \to K^+\eta'$	IV	37.4	45.2	63.2	65.6	58.8	49.0	$80^{+10}_{-9} \pm 7$
$B^0 \to K^0\eta$	IV	4.25	4.85	6.22	32.1	33.6	35.8	< 9.3
$B^0 \to K^0\eta'$	IV	36.1	44.2	63.1	64.4	57.1	46.9	$89^{+18}_{-16} \pm 9$
$B^+ \to K^+\bar{K}^0$	IV	1.59	1.84	2.41	36.4	35.9	35.2	< 5.1
$B^0 \to K^0\bar{K}^0$	IV	1.50	1.74	2.27	36.4	35.9	35.2	< 17

solid curves show the branching ratios for relevant decay modes in the SM and TC2 model. The band again refers to the corresponding CLEO data with 2σ errors, respectively: $\mathcal{B}(B \to K^+\pi^-) = (17.2^{+5.6}_{-5.4}) \times 10^{-6}$, $\mathcal{B}(B \to K^0\pi^+) = (18.2^{+9.8}_{-8.6}) \times 10^{-6}$ and $\mathcal{B}(B \to K^0\pi^0) = (14.6^{+12.8}_{-12.2}) \times 10^{-6}$. The large theoretical uncertainties are not shown in all four figures.

Although the new physics enhancements to the branching ratios of the $B \to K^+\pi$ and $K^0\pi^+$ decays are relatively large as illustrated in Figs. 2, 3 and 4, the theoretical predictions for the $B \to K\pi$ decays in the TC2 model are still consistent with the CLEO measurements within the 2σ errors after taking into account the existing large theoretical uncertainties. If one uses $F_0^{B\pi}(0) \approx 0.20$ instead of 0.33, the new physics effects will play an important role in boosting the theoretical predictions for the branching ratios of the $B \to K\pi$ decays.

4.2.2 $B \to K\eta^{(\prime)}$ decays and new physics effects

In the SM, the class-IV decays $B \to K\eta^{(\prime)}$ are expected to proceed primarily through $b \to s$ penguin diagrams and the $b \to u$ tree diagram. In the TC2 model, the new gluonic and electroweak penguins will also contribute through interference with their SM counterparts. The CLEO data of $B \to K\eta^{(\prime)}$ decays with recent measurements of $B \to \pi\pi$, $K\pi$, etc. provide important constraints on the theoretical picture for these charmless B meson decays.

For the $B^+ \to K^+\eta$ and $B^0 \to K^0\eta$ decay modes, the new physics enhancement is less than 10% for $N_c^{\rm eff} \sim 3$. The theoretical predictions in both the SM and TC2 model are consistent with the new CLEO upper limits: $\mathcal{B}(B \to K^+\eta) < 6.9 \times 10^{-6}$ and $\mathcal{B}(B \to K^0\eta) < 9.3 \times 10^{-6}$ [20].

For the $B \to K\eta'$ decay modes, the situation is very interesting now. Unexpectedly large $B \to K\eta'$ rates were firstly reported by CLEO in 1997 [52], and confirmed very recently [20,53]. The $K\eta'$ signal is large, stable and has small errors ($\sim 14\%$). Those measured ratios as given in (69) and (70) are clearly much larger than the SM predictions (the contributions from the decay $b \to s(c\bar{c}) \to s(\eta, \eta')$ have been included [13,12]) as given in Tables 3 and 4 and illustrated by the short-dashed line in Figs. 6 and 7 where only the central values of the theoretical predictions are shown. Furthermore, Lipkin's sum rule [54]

$$\mathcal{B}(K^+\eta') + \mathcal{B}(K^+\eta) = \mathcal{B}(K^+\pi^0) + \mathcal{B}(K^0\pi^+) \qquad (75)$$

is also strongly violated ($\sim 4\sigma$) [53]: $82.2^{+12.5}_{-11.6} = 29.8^{+5.7}_{-5.2}$. At present, it is indeed difficult to explain the observed large rate for $B \to K\eta'$ in the framework of the SM [20, 53]. This fact strongly suggests the requirement for additional contributions unique to the η' meson in the framework of the SM, or from new physics beyond the SM [20].

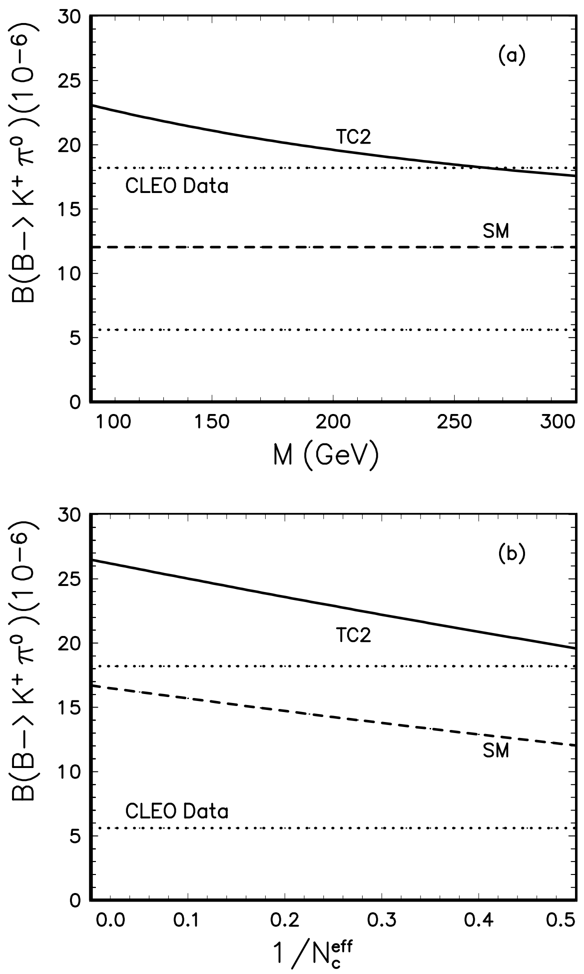

Fig. 2a,b. Plots of branching ratios of $B \to K^+\pi^0$ decay versus $m_{\tilde{\pi}}$ and $1/N_c^{\rm eff}$ in the SM and TC2 model. For **a** and **b**, we set $N_c^{\rm eff} = 2$ and $m_{\tilde{\pi}} = 200\,\mathrm{GeV}$, respectively. The short-dashed line and solid curve show the branching ratio in the SM and TC2 model, respectively. The dots band corresponds to the CLEO data with 2σ errors: $\mathcal{B}(B \to K^+\pi^0) = (11.6^{+6.6}_{-6.0}) \times 10^{-6}$

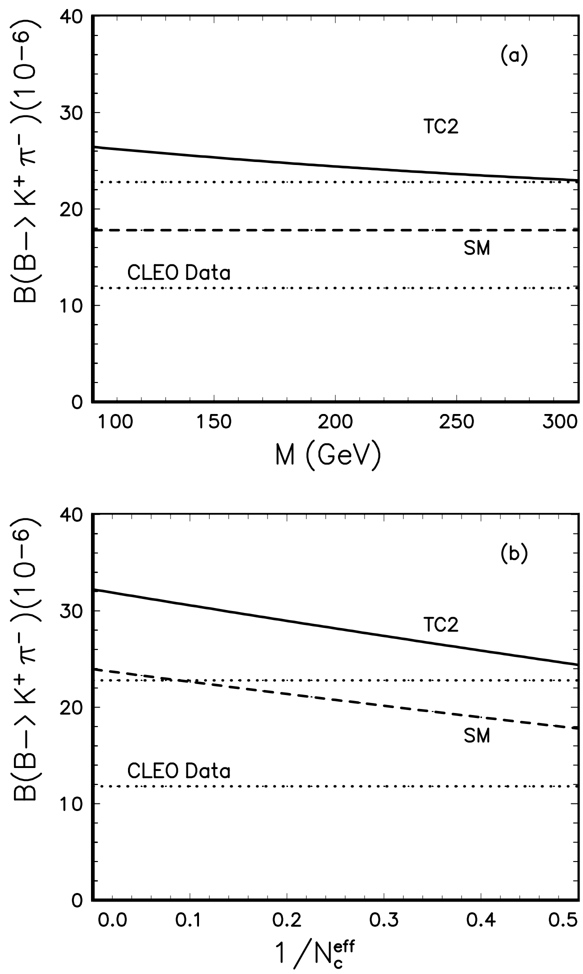

Fig. 3a,b. Same as Fig. 2 but for the case of $B \to K^+\pi^-$ decay mode. The dots band corresponds to the CLEO data with 2σ errors: $\mathcal{B}(B \to K^+\pi^-) = (17.2^{+5.6}_{-5.4}) \times 10^{-6}$

By varying η, k^2 and $m_{\tilde{\pi}}$ in the ranges of $\eta = 0.34 \pm 0.08$, $k^2 = m_b^2/2 \pm 2\,\mathrm{GeV}^2$, $m_{\tilde{\pi}} = 200 \pm 100\,\mathrm{GeV}$, and setting $N_c^{\rm eff} = 2, 3, \infty$, we find that

$$\mathcal{B}(B \to K^+\eta') = \begin{cases} (26.5 \pm 0.1^{+2.7+13.9}_{-2.2-6.9}) \times 10^{-6} \\ \quad \text{in SM}, \\ (41.6 \pm 0.1^{+6.2+17.9+3.3}_{-4.3-7.8-2.7}) \times 10^{-6} \\ \quad \text{in TC2}, \end{cases} \tag{76}$$

$$\mathcal{B}(B \to K^0\eta') = \begin{cases} (28.2 \pm 0.1^{+3.1+14.8}_{-2.1-6.3}) \times 10^{-6} \\ \quad \text{in SM}, \\ (41.3 \pm 0.1^{+6.1+19.9+3.6}_{-4.1-8.4-2.7}) \times 10^{-6} \\ \quad \text{in TC2}, \end{cases} \tag{77}$$

where the first to the fourth error corresponds to the uncertainty $\delta\eta = \pm 0.08$, $\delta q^2 = \pm 2$ and $2 \leq N_c^{\rm eff} \leq \infty$ and $\delta m_{\tilde{\pi}} = \pm 100\,\mathrm{GeV}$, respectively. If we use the LQQSR form factors instead of the BSW form factors, the central values of $BR(B \to K\eta^{(\prime)})$ will be increased by about 15%. The NP enhancements to $B \to K\eta'$ decays are significant numerically: $\sim 50\%$ for $m_{\tilde{\pi}} = 200\,\mathrm{GeV}$.

Taking into account all uncertainties considered here, the theoretical predictions for the magnitude of $B(B \to K\eta')$ in the SM and TC2 model are

$$\mathcal{B}(B \to K^+\eta') = \begin{cases} (20\text{–}53) \times 10^{-6} \\ \quad \text{in SM}, \\ (30\text{–}74) \times 10^{-6} \\ \quad \text{in TC2}, \end{cases} \tag{78}$$

$$\mathcal{B}(B \to K^0\eta') = \begin{cases} (19\text{–}52) \times 10^{-6} \\ \quad \text{in SM}, \\ (28\text{–}76) \times 10^{-6} \\ \quad \text{in TC2}, \end{cases} \tag{79}$$

It is evident that the theoretical predictions for the ratios $\mathcal{B}(B \to K\eta')$ now become consistent with the CLEO data due to the NP enhancements. This is a plausible new physics interpretation for the large $B \to K\eta'$ decay rates.

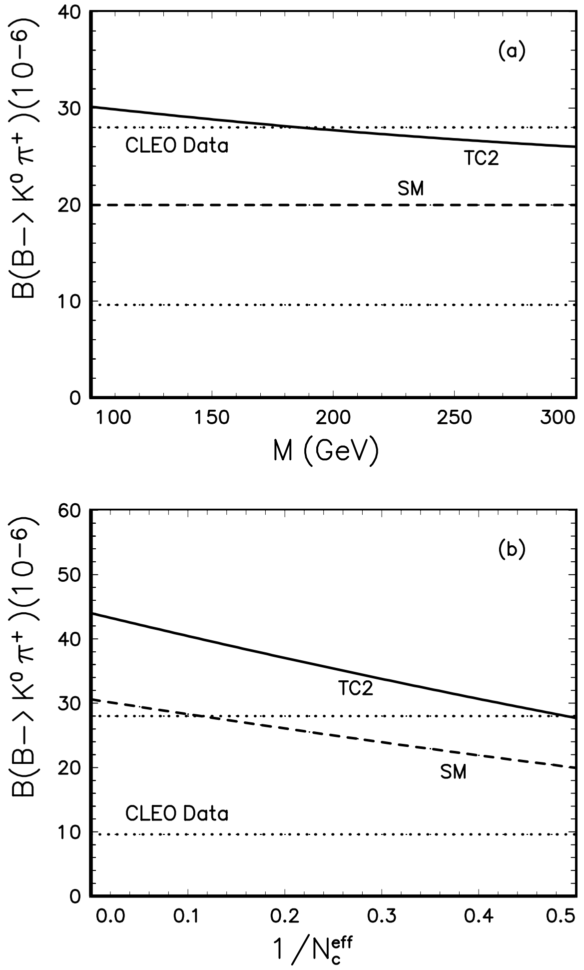

Fig. 4a,b. Same as Fig. 2 but for the case of $B \to K^0\pi^+$ decay mode. The dots band corresponds to the CLEO data with 2σ errors: $\mathcal{B}(B \to K^0\pi^+) = (18.2^{+9.8}_{-8.6}) \times 10^{-6}$

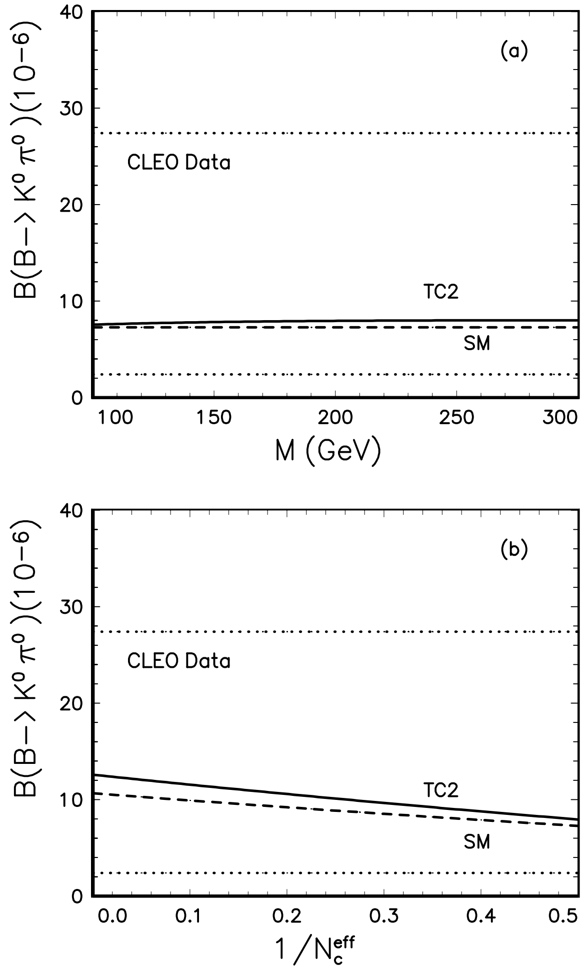

Fig. 5a,b. Same as Fig. 2 but for the case of the $B \to K^0\pi^0$ decay mode. The dotted band corresponds to the CLEO data with 1σ error: $\mathcal{B}(B \to K^0\pi^0) = (14.6^{+6.4}_{-6.1}) \times 10^{-6}$

Figures 6 and 7 show the mass and $N_c^{\rm eff}$ dependence of the ratios $B(B \to K\eta')$ in the SM and TC2 model using the input parameters as given in Appendix A and B and employing the BSW form factors. The short-dashed and solid curves in Figs. 6, 7 show the central values of theoretical predictions. The band corresponds to the CLEO measurements with 2σ errors.

4.3 Branching ratios of $B \to$ PV decays

In Tables 6–8 we present the branching ratios for the thirty-seven $B \to$ PV decay modes involving $b \to d$ and $b \to s$ transitions in the SM and TC2 model by using the BSW and LQQSR form factors and by employing generalized factorization approach. Theoretical predictions are made by using the same input parameters as those for the $B \to$ PP decays in the last subsection. The measured branching ratios from CLEO [19,20,23] for six $B \to$ PV decay modes, $B \to \rho^\pm\pi^\mp, \rho^0\pi^+$, $\omega\pi^+$, $K^{*+}\eta$, $K^{*0}\eta$, $K^{*+}\pi^-$, have been given in the last column of Table 6. BaBar and Belle also reported their measurements for $\mathcal{B}(B^0 \to \rho^-\pi^+)$ [24] and $\mathcal{B}(B \to K^\pm\phi)$ [25]:

$$\mathcal{B}(B^0 \to \rho^\pm\pi^\mp) = \begin{cases} (49 \pm 13^{+6}_{-5}) \times 10^{-6} & \text{[BaBar]}, \\ (27.6^{+8.4}_{-7.4} \pm 4.2) \times 10^{-6} & \text{[CLEO]}, \end{cases} \tag{80}$$

$$\mathcal{B}(B^\pm \to K^\pm\phi) = (17.2^{+6.7}_{-5.4} \pm 1.8) \times 10^{-6} \quad \text{[Belle]}. \tag{81}$$

The pattern $\mathcal{B}(\eta K) < \mathcal{B}(\eta K^*) < \mathcal{B}(\eta' K)$ and $\mathcal{B}(\eta' K^*) < \mathcal{B}(\eta' K)$ is found by CLEO [20].

For the considered thirty-seven $B \to$ PV decays, three general features are as follows:

(1) The theoretical predictions in the SM and TC2 model as given in Tables 6–8 are all consistent with the new experimental measurements and upper limits.
(2) For most decay modes, the differences induced by using BSW or LQQSR form factors in calculations or not are small, $\sim 15\%$.
(3) The new electroweak penguins play a more important role for $B \to$ PV decays than they do for $B \to$ PP decays.

For five $B \to \rho\pi$ and two $B \to \rho^+\eta^{(\prime)}$ decay modes, the NP contributions are very small, $< 6\%$ for $N_c^{\rm eff} = 2$–∞ as

Table 6. $B \to$ PV branching ratios (in units of 10^{-6}) using the BSW [LQQSR] form factors in the SM. The last column shows the CLEO and Belle measurements and the upper limits (90% C.L.) [19,20,25]

Channel	Class	$N_c^{\rm eff}=2$	$N_c^{\rm eff}=3$	$N_c^{\rm eff}=\infty$	Data
$B^0 \to \rho^+\pi^-$	I	21.1 [25.1]	24.0 [28.5]	30.3 [36.0]	$\}27.6^{+8.4}_{-7.4} \pm 4.2$
$B^0 \to \rho^-\pi^+$	I	5.7 [6.5]	6.48 [7.4]	8.19 [9.4]	
$B^0 \to \rho^0\pi^0$	II	0.49 [0.58]	0.06 [0.07]	2.05 [2.41]	< 5.1
$B^+ \to \rho^0\pi^+$	III	5.72 [6.63]	3.46 [3.97]	0.71 [0.78]	$10.4^{+3.3}_{-3.4} \pm 2.1$
$B^+ \to \rho^+\pi^0$	III	13.5 [16.0]	12.6 [15.0]	10.9 [13.1]	< 43
$B^0 \to \rho^0\eta$	II	0.01 [0.02]	0.02 [0.02]	0.06 [0.08]	< 10
$B^0 \to \rho^0\eta'$	II	0.02 [0.01]	0.002 [0.003]	0.03 [0.03]	< 12
$B^+ \to \rho^+\eta$	III	5.44 [6.57]	4.75 [5.79]	3.54 [4.38]	< 15
$B^+ \to \rho^+\eta'$	III	4.35 [5.02]	3.81 [4.40]	2.85 [3.29]	< 33
$B^0 \to \omega\pi^0$	II	0.29 [0.35]	0.08 [0.09]	0.15 [0.19]	< 5.5
$B^+ \to \omega\pi^+$	III	6.32 [7.35]	3.75 [4.31]	0.78 [0.85]	$11.3^{+3.3}_{-2.9} \pm 1.4$
$B^0 \to \omega\eta$	II	0.32 [0.38]	0.03 [0.04]	0.82 [0.98]	< 12
$B^0 \to \omega\eta'$	II	0.20 [0.23]	0.001 [0.002]	0.68 [0.79]	< 60
$B^0 \to \phi\pi^0$	V	0.03 [0.04]	0.002 [0.002]	0.23 [0.27]	< 5.4
$B^+ \to \phi\pi^+$	V	0.06 [0.08]	0.004 [0.005]	0.49 [0.58]	< 4
$B^0 \to \phi\eta$	V	0.01 [0.01]	0.001 [0.001]	0.09 [0.10]	< 9
$B^0 \to \phi\eta'$	V	0.01 [0.01]	0.001 [0.001]	0.07 [0.08]	< 31
$B^+ \to \bar{K}^{*0}K^+$	IV	0.42 [0.49]	0.53 [0.61]	0.78 [0.90]	< 5.3
$B^0 \to \bar{K}^{*0}K^0$	IV	0.40 [0.46]	0.50 [0.58]	0.73 [0.85]	–
$B^+ \to K^{*+}\bar{K}^0$	V	0.004 [0.006]	0.002 [0.003]	0.001 [0.001]	–
$B^0 \to K^{*0}\bar{K}^0$	IV	0.004 [0.006]	0.002 [0.003]	0.001 [0.001]	< 12
$B^0 \to \rho^0K^0$	IV	0.52 [0.60]	0.53 [0.62]	0.72 [0.83]	< 27
$B^+ \to \rho^0K^+$	IV	0.39 [0.46]	0.31 [0.36]	0.31 [0.36]	< 17
$B^0 \to \rho^-K^+$	I	0.54 [0.62]	0.59 [0.68]	0.70 [0.81]	< 25
$B^+ \to \rho^+K^0$	IV	0.11 [0.12]	0.05 [0.05]	0.005 [0.006]	< 48
$B^+ \to K^{*+}\eta$	IV	2.43 [3.12]	2.39 [3.04]	2.32 [2.89]	$26.4^{+9.6}_{-8.2} \pm 3.3$
$B^+ \to K^{*+}\eta'$	III	0.66 [1.14]	0.36 [0.61]	0.24 [0.23]	< 35
$B^0 \to K^{*0}\eta$	IV	2.32 [2.98]	2.54 [3.23]	3.06 [3.82]	$13.8^{+5.5}_{-4.6} \pm 1.6$
$B^0 \to K^{*0}\eta'$	V	0.33 [0.69]	0.09 [0.23]	0.31 [0.26]	< 20
$B^0 \to K^{*+}\pi^-$	IV	8.59 [10.2]	9.67 [11.5]	12.0 [14.3]	$22^{+8}_{-6}{}^{+4}_{-5}$
$B^0 \to K^{*0}\pi^0$	IV	2.44 [2.77]	3.02 [3.43]	4.42 [5.01]	< 3.6
$B^+ \to K^{*+}\pi^0$	IV	4.95 [6.09]	5.55 [6.84]	6.91 [8.52]	< 31
$B^+ \to K^{*0}\pi^+$	IV	7.35 [8.75]	9.23 [11.0]	13.6 [16.2]	< 16
$B^+ \to \phi K^+$	V	22.1 [25.7]	11.5 [13.4]	0.60 [0.70]	$17.2^{+6.7}_{-5.4} \pm 1.8$
$B^0 \to \phi K^0$	V	20.9 [24.3]	10.9 [12.6]	0.57 [0.66]	< 28
$B^0 \to \omega K^0$	V	3.31 [3.86]	0.002 [0.003]	13.3 [15.4]	< 21
$B^+ \to \omega K^+$	V	3.53 [4.11]	0.25 [0.28]	16.5 [19.2]	< 7.9

shown in Table 7, and can be neglected. For the $B \to \rho^0\eta$ decay, the NP enhancement can be as large as $\sim 110\%$ for $N_c^{\rm eff}=3$.

For $B \to \omega\pi$ decays, the NP contributions are small, $< 13\%$ for $N_c^{\rm eff} = 2$–∞. For $B \to \omega\eta^{(\prime)}$ decays, the NP contributions can be large but show a strong $N_c^{\rm eff}$ dependence. The agreement between the theoretical prediction and CLEO measurement for $\mathcal{B}(B \to \omega\pi^+)$ remains unchanged in the TC2 model.

For four $B \to \phi\pi, \phi\eta^{(\prime)}$ and four $B \to K^*\overline{K}$ decay modes, the NP contributions can be as large as a factor of 4, but strongly depend on $N_c^{\rm eff}$. For two $B \to \phi K$ decays, the NP enhancements are about 30% and insensitive to the variation of $N_c^{\rm eff}$. It is clear that the Belle data of $B \to K^+\phi$ [25] prefer a small effective number of colors, say $\sim N_c^{\rm eff} 2$. For four class-IV $B \to K^*\pi$ decays, the NP enhancements can be as large as 90%, and are insensitive to the variation of $N_c^{\rm eff}$.

Table 7. $B \to \mathrm{PV}$ branching ratios (in units of 10^{-6}) using the BSW [LQQSR] form factors in the TC2 model

		TC2			$\delta\mathcal{B}[\%]$		
Channel	Class	2	3	∞	2	3	∞
$B^0 \to \rho^+\pi^-$	I	21.2 [25.3]	24.1 [28.7]	30.4 [36.2]	0.71	0.63	0.50
$B^0 \to \rho^-\pi^+$	I	5.70 [6.54]	6.48 [7.44]	8.19 [9.40]	−0.06	−0.05	−0.03
$B^0 \to \rho^0\pi^0$	II	0.49 [0.58]	0.06 [0.07]	2.06 [2.43]	0.05	5.90	0.53
$B^+ \to \rho^0\pi^+$	III	5.72 [6.63]	3.46 [3.98]	0.73 [0.81]	−0.02	0.19	3.62
$B^+ \to \rho^+\pi^0$	III	13.6 [16.2]	12.7 [15.1]	11.0 [13.2]	0.83	0.86	0.92
$B^0 \to \rho^0\eta$	II	0.03 [0.04]	0.03 [0.04]	0.09 [0.11]	96.7	116	49.1
$B^0 \to \rho^0\eta'$	II	0.01 [0.01]	0.002 [0.002]	0.03 [0.03]	−21.5	−30.5	2.39
$B^+ \to \rho^+\eta$	III	5.49 [6.63]	4.82 [5.86]	3.62 [4.48]	0.96	1.29	2.26
$B^+ \to \rho^+\eta'$	III	4.35 [5.01]	3.81 [4.39]	2.85 [3.29]	−0.19	−0.08	0.15
$B^0 \to \omega\pi^0$	II	0.33 [0.39]	0.08 [0.10]	0.17 [0.21]	12.3	3.23	13.3
$B^+ \to \omega\pi^+$	III	6.58 [7.65]	3.84 [4.43]	0.78 [0.85]	4.05	2.63	−0.10
$B^0 \to \omega\eta$	II	0.38 [0.45]	0.06 [0.07]	0.82 [0.98]	19.0	107	−0.43
$B^0 \to \omega\eta'$	II	0.21 [0.24]	0.002 [0.002]	0.69 [0.79]	6.00	63.8	0.94
$B^0 \to \phi\pi^0$	V	0.03 [0.03]	0.009 [0.01]	0.37 [0.44]	−9.1	351	62.8
$B^+ \to \phi\pi^+$	V	0.06 [0.07]	0.02 [0.02]	0.79 [0.94]	−9.1	351	62.8
$B^0 \to \phi\eta$	V	0.01 [0.01]	0.003 [0.004]	0.14 [0.17]	−9.1	351	62.8
$B^0 \to \phi\eta'$	V	0.01 [0.01]	0.003 [0.003]	0.11 [0.13]	−9.1	351	62.8
$B^+ \to \bar{K}^{*0}K^+$	IV	0.64 [0.74]	0.81 [0.95]	1.22 [1.43]	52.1	54.4	57.7
$B^0 \to \bar{K}^{*0}K^0$	IV	0.60 [0.70]	0.77 [0.89]	1.16 [1.35]	52.1	54.4	57.7
$B^+ \to K^{*+}\bar{K}^0$	V	0.00 [0.002]	0.005 [0.001]	0.01 [0.01]	−71.8	−72.9	886
$B^0 \to K^{*0}\bar{K}^0$	IV	0.001 [0.002]	0.005 [0.001]	0.01 [0.01]	−71.8	−72.9	885
$B^0 \to \rho^0K^0$	IV	0.85 [0.99]	0.92 [1.07]	1.21 [1.41]	64.5	72.0	69.3
$B^+ \to \rho^0K^+$	IV	0.86 [1.00]	0.92 [1.07]	1.24 [1.44]	118	198	299
$B^0 \to \rho^-K^+$	I	0.38 [0.44]	0.45 [0.51]	0.60 [0.69]	−29.6	−24.5	−14.3
$B^+ \to \rho^+K^0$	IV	0.04 [0.04]	0.005 [0.006]	0.09 [0.11]	−66.0	−89.7	1686.
$B^+ \to K^{*+}\eta$	IV	4.02 [5.18]	3.81 [4.85]	3.39 [4.23]	65.4	59.0	46.1
$B^+ \to K^{*+}\eta'$	III	0.32 [0.55]	0.24 [0.31]	0.50 [0.44]	−50.8	−32.8	108
$B^0 \to K^{*0}\eta$	IV	3.74 [4.82]	4.07 [5.18]	4.79 [5.97]	61.4	59.8	56.6
$B^0 \to K^{*0}\eta'$	V	0.10 [0.24]	0.10 [0.08]	0.93 [0.87]	−71.3	2.18	196
$B^0 \to K^{*+}\pi^-$	IV	13.6 [16.2]	14.7 [17.5]	17.1 [20.4]	58.1	52.3	42.7
$B^0 \to K^{*0}\pi^0$	IV	2.74 [2.97]	3.58 [3.89]	5.63 [6.17]	12.5	18.5	27.4
$B^+ \to K^{*+}\pi^0$	IV	9.38 [11.7]	10.2 [12.8]	12.0 [15.1]	89.4	84.0	74.3
$B^+ \to K^{*0}\pi^+$	IV	11.2 [13.4]	14.3 [17.1]	21.6 [25.7]	53.0	55.2	58.5
$B^+ \to \phi K^+$	V	29.4 [34.3]	15.3 [17.9]	0.82 [0.95]	33.3	33.5	35.2
$B^0 \to \phi K^0$	V	27.8 [32.4]	14.5 [16.9]	0.77 [0.90]	33.3	33.5	35.2
$B^0 \to \omega K^0$	V	4.49 [5.23]	0.003 [0.003]	18.0 [21.0]	35.6	12.7	35.9
$B^+ \to \omega K^+$	V	5.18 [6.04]	0.24 [0.27]	22.8 [26.5]	46.9	−4.63	38.3

For class-I $B^0 \to \rho^-K^+$ decay, the NP correction is about −20% and insensitive to $N_c^{\rm eff}$. For $B^+ \to \rho^+K^0$ decay, however, the NP correction can be large in size, a factor of 17 enhancement for $N_c^{\rm eff} = \infty$, but very sensitive to the variation of $N_c^{\rm eff}$. For the remaining two $B \to \rho^0 K$ decays, the NP enhancements are large in size and insensitive to the value of $N_c^{\rm eff}$.

4.3.1 $B \to K^*\eta^{(\prime)}$ decays

Very recently, CLEO reported the first observation [20] of $B \to K^*\eta$ decays:

$$\mathcal{B}(B^+ \to K^{*+}\eta) = (26.4^{+9.6}_{-8.2} \pm 3.3) \times 10^{-6}, \quad (82)$$

$$\mathcal{B}(B^0 \to K^{*0}\eta) = (13.8^{+5.5}_{-4.6} \pm 1.6) \times 10^{-6}, \quad (83)$$

Table 8. $B \to$ PV branching ratios (in units of 10^{-6}) using the BSW form factors in TC2 model with new contributions induced by charged-Higgs gluonic penguin diagrams only

		TC2: QCD only			$\delta\mathcal{B}[\%]$		
Channel	Class	2	3	∞	2	3	∞
$B^0 \to \rho^+\pi^-$	I	21.2	24.1	30.4	0.64	0.62	0.59
$B^0 \to \rho^-\pi^+$	I	5.70	6.48	8.19	−0.06	−0.05	−0.04
$B^0 \to \rho^0\pi^0$	II	0.54	0.11	2.12	9.68	95.0	3.12
$B^+ \to \rho^0\pi^+$	III	5.77	3.52	0.78	0.94	1.75	10.6
$B^+ \to \rho^+\pi^0$	III	13.6	12.7	11.0	0.32	0.38	0.54
$B^0 \to \rho^0\eta$	II	0.03	0.03	0.08	105	115	41.1
$B^0 \to \rho^0\eta'$	II	0.004	0.003	0.04	−51.1	−9.35	25.5
$B^+ \to \rho^+\eta$	III	5.47	4.79	3.59	0.61	0.82	1.44
$B^+ \to \rho^+\eta'$	III	4.34	3.81	2.86	−0.21	0.0	0.56
$B^0 \to \omega\pi^0$	II	0.43	0.13	0.15	46.8	70.6	−1.97
$B^+ \to \omega\pi^+$	III	6.59	3.85	0.77	4.33	2.87	−0.41
$B^0 \to \omega\eta$	II	0.37	0.05	0.82	16.0	73.8	−0.08
$B^0 \to \omega\eta'$	II	0.23	0.006	0.68	13.6	363	−0.89
$B^0 \to \phi\pi^0$	V	0.04	0.002	0.30	39.6	13.5	32.2
$B^+ \to \phi\pi^+$	V	0.09	0.005	0.64	39.6	13.5	32.2
$B^0 \to \phi\eta$	V	0.02	0.001	0.11	39.6	13.5	32.2
$B^0 \to \phi\eta'$	V	0.01	0.001	0.09	39.6	13.5	32.2
$B^+ \to \bar{K}^{*0}K^+$	IV	0.65	0.79	1.13	54.9	51.0	45.2
$B^0 \to \bar{K}^{*0}K^0$	IV	0.61	0.75	1.07	54.9	51.0	45.2
$B^+ \to K^{*+}\bar{K}^0$	V	0.001	0.001	0.005	−87.0	−68.2	519
$B^0 \to K^{*0}\bar{K}^0$	IV	0.001	0.001	0.005	−87.0	−68.2	519
$B^0 \to \rho^0K^0$	IV	0.34	0.35	0.52	−34.9	−34.9	−27.6
$B^+ \to \rho^0K^+$	IV	0.47	0.41	0.47	19.0	33.8	51.5
$B^0 \to \rho^-K^+$	I	0.41	0.47	0.58	−23.8	−21.5	−17.8
$B^+ \to \rho^+K^0$	IV	0.02	0.005	0.05	−84.4	−90.4	907
$B^+ \to K^{*+}\eta$	IV	2.96	2.95	2.96	21.6	23.5	27.3
$B^+ \to K^{*+}\eta'$	III	0.27	0.34	0.86	−59.3	−5.79	260
$B^0 \to K^{*0}\eta$	IV	2.84	3.13	3.78	22.6	23.0	23.5
$B^0 \to K^{*0}\eta'$	V	0.08	0.27	1.23	−75.7	188	292
$B^0 \to K^{*+}\pi^-$	IV	13.1	14.7	18.1	52.5	51.7	50.2
$B^0 \to K^{*0}\pi^0$	IV	4.09	4.93	6.90	67.8	63.3	56.1
$B^+ \to K^{*+}\pi^0$	IV	7.15	8.02	9.96	44.5	44.4	44.1
$B^+ \to K^{*0}\pi^+$	IV	11.5	14.0	19.9	55.8	51.7	45.8
$B^+ \to \phi K^+$	V	33.4	17.9	1.31	51.2	55.9	118
$B^0 \to \phi K^0$	V	31.6	16.9	1.24	51.2	55.9	118
$B^0 \to \omega K^0$	V	5.07	0.01	17.4	53.1	489	31.0
$B^+ \to \omega K^+$	V	5.31	0.22	21.2	50.3	−10.2	28.7

while the theoretical predictions in the SM and TC2 model are

$$\mathcal{B}(B^+ \to K^{*+}\eta) = \begin{cases} (1.5\text{–}3.8) \times 10^{-6} \\ \quad \text{in SM}, \\ (1.9\text{–}6.1) \times 10^{-6} \\ \quad \text{in TC2}, \end{cases} \tag{84}$$

$$\mathcal{B}(B^+ \to K^{*0}\eta) = \begin{cases} (1.5\text{–}4.5) \times 10^{-6} \\ \quad \text{in SM}, \\ (2.3\text{–}7.2) \times 10^{-6} \\ \quad \text{in TC2}, \end{cases} \tag{85}$$

where the uncertainties induced by using the BSW or LQQSE form factors, and setting $k^2 = m_b^2/2 \pm 2\,\mathrm{GeV}^2$, $\eta = 0.34 \pm 0.08$, $N_c^{\mathrm{eff}} = 2$–∞, and $m_{\tilde{\pi}} = 200 \pm 100\,\mathrm{GeV}$, have been taken into account. Although the central values of the theoretical predictions for $\mathcal{B}(B \to K^*\eta)$ decays are much smaller than the central values of the data, the theoretical predictions are still consistent with the data since the experimental errors are still rather large. Further refinement of the data will show whether there is a real difference between the data and theoretical predictions.

The new physics enhancements to the decay rates are significant ($\sim 60\%$) in size, insensitive to variation of N_c^{eff} and hence helpful to improve the agreement between the

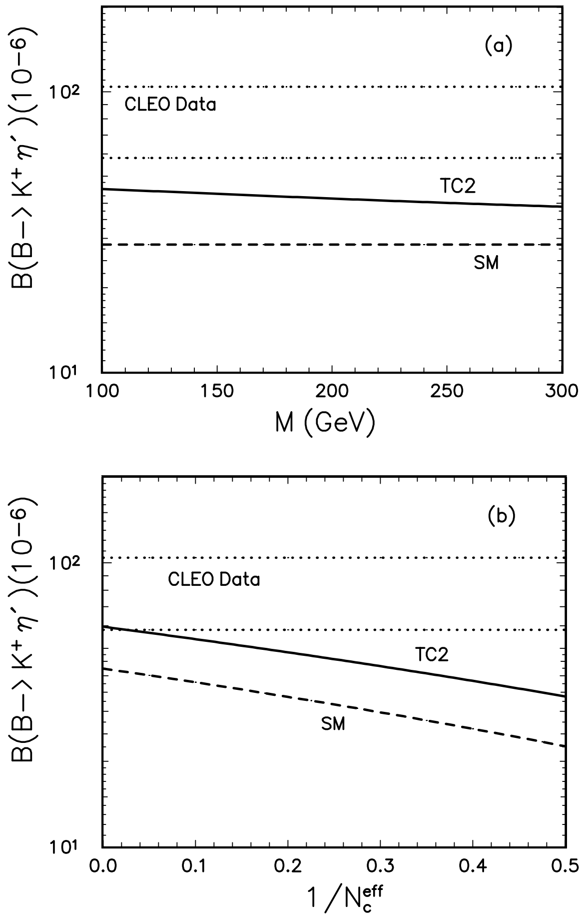

Fig. 6a,b. Plots of the branching ratios of the decays $B^+ \to K^+\eta'$ versus $m_{\tilde{\pi}}$ and $1/N_c^{\rm eff}$ in the SM and TC2 model. For (a) and (b), we set $N_c^{\rm eff} = 3$ and $m_{\tilde{\pi}} = 200\,$GeV, respectively. The short-dashed line (solid curve) shows $\mathcal{B}(B^+ \to K^+\eta')$ in the SM (TC2 model). The dotted band corresponds to the CLEO data with 2σ errors: $\mathcal{B}(B^+ \to K^+\eta') = (80^{+24}_{-22}) \times 10^{-6}$

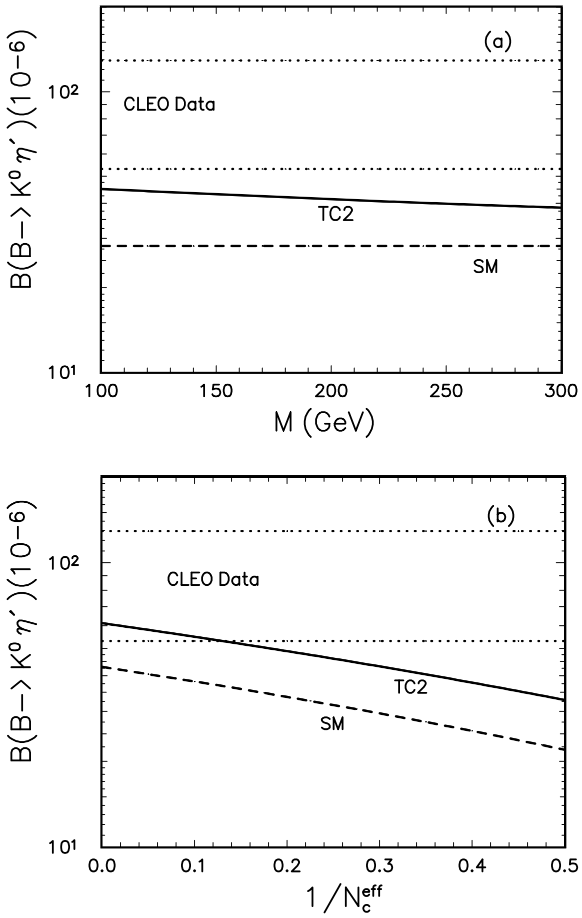

Fig. 7a,b. Same as Fig. 6 but for the $B^0 \to K^0\eta'$ decay. The dotted band corresponds to the CLEO data with 2σ errors: $\mathcal{B}(B^0 \to K^0\eta') = (89^{+40}_{-36}) \times 10^{-6}$

theoretical predictions and the data, as illustrated in Figs. 8 and 9 where the upper dots band shows the CLEO data [19,20].

Figures 8 and 9 show the mass and $N_c^{\rm eff}$ dependence of the decay rates $\mathcal{B}(B^+ \to K^{*+}\eta)$ and $\mathcal{B}(B^+ \to K^{*0}\eta)$, respectively. For Figs. 8a and 9a, we set $N_c^{\rm eff} = 3$. For Figs.8b and 9b, we set $m_{\tilde{\pi}} = 200\,$GeV. In these two figures, the dot-dashed line refers to the SM prediction, while the short-dashed (the solid curve) corresponds to the theoretical prediction with the inclusion of NP effects from new gluonic (both gluonic and electroweak) penguins. It is clear that the electroweak penguin play an important role for these two decay modes.

For other two $B \to K^*\eta'$ decays, the new physics enhancement can be significant in size, from -70% to $\sim 200\%$, but strongly depend on the variation of $N_c^{\rm eff}$, as shown in Table 7. The theoretical predictions for these two decay modes are still far below the current CLEO upper limits.

5 CP-violating asymmetries in $B \to$ PP, PV decays

As is well known, there are three possible manifestations of CP-violation in the B system [1,28,55,56]: the direct CP-violation or CP-violation in decay, the indirect CP-violation or CP-violation in mixing due to the interference between mixing amplitudes, and finally the CP-violation in interference between decays with and without mixing. For the measurements of CP-violation in the B system, great progress has been achieved recently [22,57].

In [26], Ali et al. estimated the CP-violating asymmetries in charmless hadronic decays $B \to$ PP, PV, VV, based on the effective Hamiltonian with generalized factorization. In another paper [58], Chen et al. calculated the CP-violating asymmetries in charmless hadronic decays of the B_s meson. We here will follow the same procedure as in [26] to estimate the new physics effects on the CP-violating asymmetries of $B \to$ PP, PV decays in the TC2 model.

In TC2 model, no new weak phase has been introduced through the interactions involving new particles and hence the mechanism of CP-violation in TC2 model is the same as in the SM. But the CP-violating asymmetries

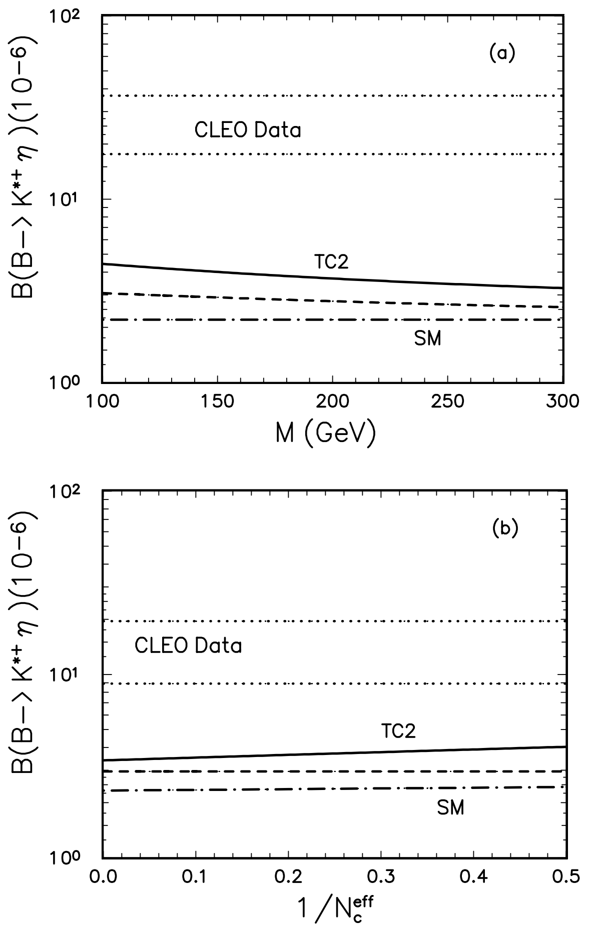

Fig. 8a,b. Plots of $\mathcal{B}(B^+ \to K^{*+}\eta)$ versus $m_{\tilde{\pi}}$ and $1/N_c^{\rm eff}$ in the SM and TC2 model. For **a** and **b**, we set $N_c^{\rm eff} = 3$ and $m_{\tilde{\pi}} = 200\,\mathrm{GeV}$, respectively. The dot-dashed line shows the SM prediction, while the short-dashed and solid curve refer to the ratios with the inclusion of contributions induced by new gluonic penguins and both new gluonic and electroweak penguins, respectively. The upper band corresponds to the CLEO data with 1σ error: $\mathcal{B}(B^+ \to K^{*+}\eta) = (26.4^{+10.2}_{-8.8}) \times 10^{-6}$

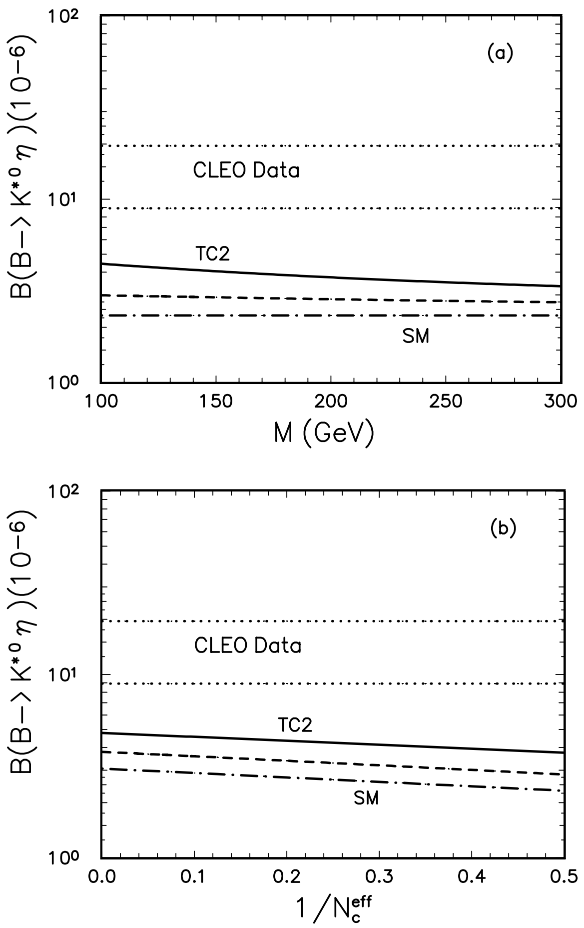

Fig. 9a,b. Same as Fig. 8, but for the decay $\mathcal{B}(B^0 \to K^{*0}\eta)$. The upper band corresponds to the CLEO data with 1σ error: $\mathcal{B}(B^0 \to K^{*0}\eta) = (13.8^{+5.7}_{-4.9}) \times 10^{-6}$

$\mathcal{A}_{CP}$ may be changed by the inclusion of new physics contributions through the interference between the ordinary tree/penguin amplitudes in the SM and the new strong and electroweak penguin amplitudes in TC2 model. The real and imaginary part of effective Wilson coefficients $C_i^{\rm eff}$ and effective number a_i will be modified by new physics effects and hence the pattern of $\mathcal{A}_{CP}$ for two-body charmless hadronic B decays will be changed accordingly.

5.1 Formalism

For charged B decays the direct CP-violation is defined by

$$\mathcal{A}_{CP} = \frac{\Gamma(B^+ \to f) - \Gamma(B^- \to \bar{f})}{\Gamma(B^+ \to f) + \Gamma(B^- \to \bar{f})} \tag{86}$$

in terms of partial decay widths.

For neutral $B^0(\bar{B}^0)$ decays, the situation becomes complicated because of B^0–$\bar{B}^0$ mixing, and hence the time dependent CP-asymmetry for the decays of states that were tagged as pure B^0 or $\bar{B}^0$ at production is defined by

$$\mathcal{A}_{CP}(t) = \frac{\Gamma(B^0(t) \to f) - \Gamma(\bar{B}^0(t) \to \bar{f})}{\Gamma(B^0(t) \to f) + \Gamma(\bar{B}^0(t) \to \bar{f})}. \tag{87}$$

According to the characteristics of the final states f, neutral B decays can be classified into four cases as described in [26]. For case-1, f or $\bar{f}$ is not a common final state of B^0 and $\bar{B}^0$, and the CP-violating asymmetry is independent of time. We use (86) to calculate the CP-violating asymmetries for CP-class-1 decays: the charged B and case-1 neutral B decays.

For CP-class-2 (class-3) B decays where $\overset{(-)}{B^0} \to (f = \bar{f})$ with $f^{CP} = \pm f$ ($f^{CP} \neq \pm f$) [26], the time dependent and time-integrated CP-asymmetries are of the form

$$\mathcal{A}_{CP}(t) = a_{\epsilon'} \cos(\Delta m t) + a_{\epsilon+\epsilon'} \sin(\Delta m t), \tag{88}$$

$$\mathcal{A}_{CP} = \frac{1}{1+x^2} a_{\epsilon'} + \frac{x}{1+x^2} a_{\epsilon+\epsilon'}, \tag{89}$$

where $\Delta m = m_H - m_{\rm L}$ is the mass difference between the mass eigenstates $|B_H^0\rangle$ and $|B_{\rm L}^0\rangle$, $x = \Delta m/\Gamma \approx 0.73$ for the case of B_d^0–$\bar{B}_d^0$ mixing [42], and

$$a_{\epsilon'} = \frac{1-|\lambda_{CP}|^2}{1+|\lambda_{CP}|^2}, \quad a_{\epsilon+\epsilon'} = \frac{-2\mathrm{Im}(\lambda_{CP})}{1+|\lambda_{CP}|^2}, \tag{90}$$

$$\lambda_{CP} = \frac{V_{tb}^* V_{td}}{V_{tb} V_{td}^*} \frac{\langle f|H_{\mathrm{eff}}|\bar{B}^0\rangle}{\langle f|H_{\mathrm{eff}}|B^0\rangle}. \tag{91}$$

For the formulae used to calculate $\mathcal{A}_{CP}$ for the more complicated CP-class-4 B decays, see (36)–(40) of [26]. We also define the ratio

$$\delta\mathcal{A}_{CP} = \frac{\mathcal{A}_{CP}^{\mathrm{TC2}} - \mathcal{A}_{CP}^{\mathrm{SM}}}{\mathcal{A}_{CP}^{\mathrm{SM}}} \tag{92}$$

to measure the new physics effects on the SM predictions of $\mathcal{A}_{CP}$ of the B meson decays.

As an example, we here present the explicit calculation for the class-III-1 decay $B^\pm \to \pi^\pm\pi^0$. The decay amplitude $M(B^- \to \pi^-\pi^0)$ has been given in (59) where all a_i should be taken for transitions $b \to d$. For the charged conjugate amplitude we have

$$\begin{aligned} M(B^+ \to \pi^+\pi^0) &= -\mathrm{i}\frac{G_{\mathrm{F}}}{2} f_\pi F_0^{B\to\pi}(m_\pi^2)(m_B^2 - m_\pi^2) \\ &\times \Big\{ V_{ub}^* V_{ud}(a_1 + a_2) \\ &- V_{tb}^* V_{td} \times \frac{3}{2}(-a_7 + a_9 + a_{10} + a_8 R_2) \Big\}, \end{aligned} \tag{93}$$

where the ratio R_2 has been given in (56), and all a_i are taken for transitions $\bar{b} \to \bar{d}$. The CP-asymmetry for this decay mode is then defined by

$$\begin{aligned} &\mathcal{A}_{CP}(B^\pm \to \pi^\pm\pi^0) = \\ &\frac{|M(B^+ \to \pi^+\pi^0)|^2 - |M(B^- \to \pi^-\pi^0)|^2}{|M(B^+ \to \pi^+\pi^0)|^2 + |M(B^- \to \pi^-\pi^0)|^2}. \end{aligned} \tag{94}$$

5.2 Numerical results

In Tables 9–14, we present numerical results of $\mathcal{A}_{CP}$ in $B \to \mathrm{PP}$ and $B \to \mathrm{PV}$ decays in the SM and TC2 model. We show the numerical results for the case of using BSW form factors only since the form factor dependence is weak. In the second column of Tables 9–14, roman numbers and arabic numbers denote the classification of the decays $B \to \mathrm{PP}, \mathrm{PV}$ using the N_c^{eff} dependence and the CP-class for each decay mode as defined in [12, 26], respectively. The first and second error of the theoretical predictions correspond to the uncertainties induced by setting $\delta k^2 = \pm 2\,\mathrm{GeV}^2$ and $\delta\eta = \pm 0.08$, respectively.

The SM predictions for the CP-violating asymmetries of fifty-seven B meson decay modes investigated here as given in Tables 9–14 are well consistent with those given in [26]. For details of the parametric dependence of $\mathcal{A}_{CP}$ in the SM, see [26]. We here focus on the new physics effects on $\mathcal{A}_{CP}$ of the B meson decays.

Very recently, CLEO reported their first measurements of CP-violating asymmetries for the five decay modes [22], $B^\pm \to K^\pm\pi^0, K_S^0\pi^\pm, \omega\pi^\pm$ and $\overset{(-)}{B^0} \to K^\pm\pi^\mp$. They conclude that the measured asymmetries are consistent with zero in all five decay modes studied [22].

Using the same input parameters as in Table 9, we find the theoretical predictions in the TC2 model for those five decay modes

$$\mathcal{A}_{CP}(B \to K^\pm\pi^0) = (-3.4^{+1.6}_{-0.9} \pm 0.8^{+0.7+0.4}_{-0.4-0.3}) \times 10^{-2}, \tag{95}$$

$$\mathcal{A}_{CP}(B \to K^\pm\pi^\mp) = (-5.0^{+2.5}_{-1.5} \pm 1.1^{+0.1+0.3}_{-0.2-0.2}) \times 10^{-2}, \tag{96}$$

$$\mathcal{A}_{CP}(B \to K_S^0\pi^\mp) = (-1.1 \pm 0.1^{+0.2}_{-0.1} \pm 0.1 \pm 0.1) \times 10^{-2}, \tag{97}$$

$$\mathcal{A}_{CP}(B \to K^\pm\eta') = (-2.8^{+1.0}_{-0.6} \pm 0.7^{+0.8}_{-0.5} \pm 0.1) \times 10^{-2}, \tag{98}$$

$$\mathcal{A}_{CP}(B \to \omega\pi^\pm) = (8.9 \pm 0.1^{+0.4+1.7}_{-0.7-11.1} \pm 0.1) \times 10^{-2}, \tag{99}$$

where the central values correspond to setting $k^2 = m_b^2/2$, $\eta = 0.34$ and $N_c^{\mathrm{eff}} = 3$, while the first to fourth error is induced by considering the uncertainty $\delta k^2 = \pm 2\,\mathrm{GeV}^2$, $\delta\eta = \pm 0.8$, $2 \le N_c^{\mathrm{eff}} \le \infty$ and $\delta m_{\tilde{\pi}} = \pm 100\,\mathrm{GeV}$, respectively. For the first four $B \to \mathrm{PP}$ decay modes, the uncertainty induced by varying N_c^{eff} is smaller or comparable in size with the other three uncertainties. For the $B \to \omega\pi^\pm$ decay mode, however, the uncertainty induced by varying N_c^{eff} dominates over the other three uncertainties.

The CLEO measurements, the 90% CL region and the theoretical predictions in the SM and TC2 model are as given in Table 15. The theoretical predictions are taken from Tables 9–14 and (95)–(99). One also should note that the sign convention used here in (86) and (87) to define $\mathcal{A}_{CP}$ is opposite to that used in [22]; we therefore changed the sign of the theoretical predictions of $\mathcal{A}_{CP}$ in Table 15 in order to be consistent with the results reported by CLEO.

It is easy to see that the CP-violating asymmetries of all five decay modes studied are small in size in both the SM and the TC2 model, and well consistent with the CLEO data. For all five decay modes, the new physics corrections are also small; this will change the SM predictions by about 20%. Figure 10 and 11 show the mass and N_c^{eff} dependence for $B^\pm \to K^\pm\eta'$ and $B^\pm \to \omega\pi^\pm$ in the SM (the dotted lines or curves) and TC2 model (the solid curves)[5]

From the theoretical predictions and the CLEO measurements as given in Tables 9–15, the following general features of the CP-violating asymmetry of the charmless hadronic B meson decays under study in this paper can be understood:

(1) The CP-violating asymmetries depend weakly on whether we use the BSW or LQQSR form factors. The inclusion of NP contributions does not change this feature.

[5] In these two figures we use the same sign convention as the CLEO Collaboration [22]

Table 9. CP-violating asymmetries $\mathcal{A}_{CP}$ in $B \to \mathrm{PP}$ decays (in percent) in the SM using $\rho = 0.12$ and $N_c^{\mathrm{eff}} = 2, 3, \infty$ for $k^2 = m_b^2/2 \pm 2\,\mathrm{GeV}^2$ and $\eta = 0.34 \pm 0.8$. The first and second error of the ratios corresponds to $\delta k^2 = \pm 2\,\mathrm{GeV}^2$ and $\delta\eta = \pm 0.08$, respectively

Channel	Class	2	3	∞
$\overset{(-)}{B^0} \to \pi^+\pi^-$	I-2	$23.7^{+0.3+16.2}_{-1.3-15.9}$	$23.4^{+0.3+16.5}_{-1.2-15.9}$	$23.0^{+0.3+16.6}_{-1.2-15.9}$
$\overset{(-)}{B^0} \to \pi^0\pi^0$	II-2	$-54.9^{+9.5+1.0}_{-3.9-1.2}$	$15.3^{+6.1+2.6}_{-3.4-3.0}$	$48.0^{+1.0+7.8}_{-2.9-12.7}$
$B^\pm \to \pi^\pm\pi^0$	III-1	$0.1^{+0.01+0.02}_{-0.02-0.01}$	$0.1^{+0.01+0.02}_{-0.02-0.01}$	$0.$
$\overset{(-)}{B^0} \to \eta\eta$	II-2	$57.5^{+1.5+2.7}_{-2.5-7.2}$	$13.8^{+4.7+2.3}_{-2.6-2.8}$	$-53.1^{+6.9+0.7}_{-2.9-1.5}$
$\overset{(-)}{B^0} \to \eta\eta'$	II-2	$60.8^{+2.0-4.2}_{-4.3-0.7}$	$20.0^{+5.9+3.5}_{-3.3-4.0}$	$-52.6^{+6.9+0.4}_{-2.9-1.5}$
$\overset{(-)}{B^0} \to \eta'\eta'$	II-2	$44.8^{+1.4+14.4}_{-5.2-16.3}$	$36.2^{+7.6+6.0}_{-4.8-7.2}$	$-47.3^{+6.5+0.7}_{-1.9-1.4}$
$B^\pm \to \pi^\pm\eta$	III-1	$12.1^{+2.4+0.3}_{-5.2-0.2}$	$14.3^{+2.7+0.3}_{-5.6-1.2}$	$18.1^{+2.7+2.6}_{-5.0-3.3}$
$B^\pm \to \pi^\pm\eta'$	III-1	$12.6^{+2.9+0.9}_{-6.3-1.2}$	$15.5^{+3.4+0.3}_{-7.2-0.9}$	$22.4^{+4.2+1.4}_{-8.0-2.7}$
$\overset{(-)}{B^0} \to \pi^0\eta$	V-2	$28.5^{+2.8+5.2}_{-1.5-5.8}$	$14.3^{+5.1+2.4}_{-2.8-2.9}$	$-9.9^{+8.2+1.7}_{-4.5-1.3}$
$\overset{(-)}{B^0} \to \pi^0\eta'$	V-2	$53.5^{+0.3+8.4}_{-0.1-10.3}$	$24.9^{+7.2+4.2}_{-4.2-5.0}$	$-16.8^{+13+2.6}_{-7.7-1.9}$
$B^\pm \to K^\pm\pi^0$	IV-1	$-5.6^{+2.9+1.2}_{-1.6-1.2}$	$-5.0^{+2.5+1.2}_{-1.3-1.0}$	$-3.8^{+1.7+0.9}_{-1.0-0.9}$
$\overset{(-)}{B^0} \to K^\pm\pi^\mp$	IV-1	$-6.1^{+3.2+1.4}_{-1.7-1.3}$	$-6.2^{+3.2+1.4}_{-1.8-1.3}$	$-6.4^{+3.4}_{-1.8} \pm 1.4$
$B^\pm \to K_S^0\pi^\pm$	IV-1	$-1.3 \pm 0.1 \pm 0.3$	$-1.2 \pm 0.1 \pm 0.3$	$-1.2 \pm 0.1 \pm 0.3$
$\overset{(-)}{B^0} \to K_S^0\pi^0$	IV-2	$34.4^{+0.3+5.0}_{-0.6-6.4}$	$31.2 \pm 0.0^{+4.8}_{-5.9}$	$25.6^{+0.9+4.1}_{-0.6-5.0}$
$B^\pm \to K^\pm\eta$	IV-1	$4.0^{+1.7+0.8}_{-3.3-0.9}$	$2.9^{+1.4+0.7}_{-2.5-0.6}$	$1.0^{+0.8}_{-1.3} \pm 0.2$
$B^\pm \to K^\pm\eta'$	IV-1	$-4.4^{+1.9+1.0}_{-1.1-1.1}$	$-3.6^{+1.4}_{-0.8} \pm 0.8$	$-2.5^{+0.7}_{-0.4} \pm 0.5$
$\overset{(-)}{B^0} \to K_S^0\eta$	IV-2	$34.7^{+0.4+5.0}_{-0.6-6.4}$	$30.9 \pm 0.0^{+4.7}_{-5.9}$	$23.7^{+1.2+3.9}_{-0.7-4.6}$
$\overset{(-)}{B^0} \to K_S^0\eta'$	IV-2	$29.7^{+0.3+4.7}_{-0.2-5.7}$	$31.2 \pm 0.0^{+4.8}_{-5.9}$	$33.2^{+0.2+5.0}_{-0.3-6.2}$
$B^\pm \to K^\pm\bar{K}_S^0$	IV-1	$10.5^{+5.1+1.9}_{-2.6-2.2}$	$10.4^{+5.0+1.8}_{-2.5-2.2}$	$10.2^{+5.0+1.8}_{-2.6-2.1}$
$\overset{(-)}{B^0} \to K^0\bar{K}^0$	IV-2	$13.5^{+5.0+2.3}_{-2.6-2.7}$	$13.4^{+4.9+2.2}_{-2.7-2.7}$	$13.1^{+4.9+2.3}_{-2.6-2.6}$

(2) The $m_{\tilde{\pi}}$ dependence of $\mathcal{A}_{CP}$ is weak: $\delta\mathcal{A}_{CP}$ is about $\pm 15\%$ as one varies $m_{\tilde{\pi}}$ in the range $100\,\mathrm{GeV} \leq m_{\tilde{\pi}} \leq 300\,\mathrm{GeV}$.
(3) For twenty $B \to \mathrm{PP}$ decays, the new physics corrections to $\mathcal{A}_{CP}$ are generally small or moderate in magnitude. The largest correction is about -30% for the decay $B^\pm \to K^\pm\pi^0$, and about $\pm 20\%$ for the decay modes $\overset{(-)}{B^0} \to \pi^+\pi^-, \pi^0\eta, K^+\pi^-, K^0\bar{K}^0$ and $B^+ \to K^0\pi^+, K^0\bar{K}^0$. For four class-II $B \to \eta\eta^{(\prime)}, \eta'\eta'$ and $\pi^0\pi^0$ decays, there are large CP-violating asymmetries (around $\pm 50\%$), but unfortunately there is also a strong N_c^{eff} dependence in both the SM and the TC2 model.
(4) For the $B \to \mathrm{PV}$ decays, however, the NP corrections to $\mathcal{A}_{CP}$ can be rather large for many decay modes, as illustrated in Table 13. For class-I-4 decay $B^0/\bar{B}^0 \to \rho^+\pi^-/\rho^-\pi^+$, the new physics correction is $(60 \sim 100)\%$ for $N_c^{\mathrm{eff}} = 2$–∞. For the decay $B^+ \to K^{*+}\bar{K}^0$ the correction even reaches a factor of 20 for $N_c^{\mathrm{eff}} = 2$ due to strong interference between the contributions from the $W-$penguin and new charged-scalar penguins.
(5) For most class-I, III and IV decays, the N_c^{eff} dependence and k^2 dependence of $\delta\mathcal{A}_{CP}$ are weak. For most class-V decays, however, the N_c^{eff} dependence of $\delta\mathcal{A}_{CP}$ is strong.
(6) For most decay modes considered here, the new physics corrections to $\mathcal{A}_{CP}$ in the TC2 model are still much smaller than the existing theoretical uncertainties, and therefore will be masked by the latter. Low experimental statistics and large theoretical uncertainties together prevent us from testing the TC2 model through studies of the CP-violating asymmetries at present.

According to the relevant studies [59] for these decay modes, we know that the FSI may provide a new strong phase and therefore enhance $\mathcal{A}_{CP}$ to a level 20%–40%; new physics with new large phases may also increase $\mathcal{A}_{CP}$ to a level of 40%–60%. Although there is still no evidence for direct CP-violation in the B system, the CLEO measurements ruled out a large part of the parameter space for $\mathcal{A}_{CP}$. The key problem is that the measurements are currently statistics limited.

6 Summary and discussions

In this paper, we calculated the new physics contributions to the branching ratios and CP-violating asymmetries of the two-body charmless hadronic B meson decays $B \to \mathrm{PP}, \mathrm{PV}$ in the TC2 model by employing the NLO effective Hamiltonian with generalized factorization. We

Table 10. Same as in Table 9 but in the TC2 model and assuming $m_{\tilde{\pi}} = 200\,\text{GeV}$

		TC2			$\delta\mathcal{A}_{CP}[\%]$		
Channel	Class	2	3	∞	2	3	∞
$\overset{(-)}{B^0} \to \pi^+\pi^-$	I-2	27.3	26.9	26.3	15.3	14.9	14.3
$\overset{(-)}{B^0} \to \pi^0\pi^0$	II-2	−55.5	14.9	49.8	1.0	−2.9	3.7
$B^\pm \to \pi^\pm\pi^0$	III-1	0.07	0.05	0.0	0.4	0.4	−
$\overset{(-)}{B^0} \to \eta\eta$	II-2	51.9	10.7	−50.9	−9.9	−22.4	−4.2
$\overset{(-)}{B^0} \to \eta\eta'$	II-2	60.4	15.4	−53.7	−0.7	−23.2	2.0
$\overset{(-)}{B^0} \to \eta'\eta'$	II-2	55.3	27.5	−50.7	23.3	−24.0	7.2
$B^\pm \to \pi^\pm\eta$	III-1	12.0	13.7	15.7	−0.7	−4.0	−13.5
$B^\pm \to \pi^\pm\eta'$	III-1	13.1	15.9	21.5	4.3	2.4	−4.1
$\overset{(-)}{B^0} \to \pi^0\eta$	V-2	23.8	11.8	−7.9	−16.3	−17.1	−19.8
$\overset{(-)}{B^0} \to \pi^0\eta'$	V-2	46.2	21.3	−14.8	−13.7	−14.2	−12.3
$B^\pm \to K^\pm\pi^0$	IV-1	−3.8	−3.4	−2.7	−31.8	−30.8	−28.9
$\overset{(-)}{B^0} \to K^\pm\pi^\mp$	IV-1	−4.8	−5.0	−5.2	−20.5	−20.0	−19.1
$B^\pm \to K^0_S\pi^\pm$	IV-1	−1.2	−1.1	−1.0	−15.0	−15.6	−16.4
$\overset{(-)}{B^0} \to K^0_S\pi^0$	IV-2	34.3	31.3	26.1	−0.2	0.2	2.1
$B^\pm \to K^\pm\eta$	IV-1	4.11	2.7	0.9	3.5	−3.6	−16.7
$B^\pm \to K^\pm\eta'$	IV-1	−3.34	−2.8	−2.0	−24.6	−22.4	−18.8
$\overset{(-)}{B^0} \to K^0_S\eta$	IV-2	35.2	31.3	24.7	1.2	1.5	4.1
$\overset{(-)}{B^0} \to K^0_S\eta'$	IV-2	30.1	31.2	32.9	1.1	0.04	−1.0
$B^\pm \to K^\pm\bar{K}^0_S$	IV-1	8.8	8.6	8.3	−16.4	−17.0	−18.0
$\overset{(-)}{B^0} \to K^0\bar{K}^0$	IV-2	11.5	11.3	10.9	−15.2	−15.8	−16.7

will present the calculation for the new physics effects on $\mathcal{B}(B \to \text{VV})$ and $\mathcal{A}_{CP}(B \to \text{VV})$ in a forthcoming paper [60]

We firstly evaluate analytically all strong and electroweak charged-scalar penguin diagrams in the quark level processes $b \to sV^*$ with $V = \gamma, \text{gluon}, Z$, extract the corresponding Inami–Lim functions $C_0^{\text{TC2}}, D_0^{\text{TC2}}, E_0^{\text{TC2}}$ and $C_{\text{g}}^{\text{TC2}}$ which describe the NP contributions to the Wilson coefficients $C_i(M_W)$ ($i = 3$–10) and $C_{\text{g}}(M_W)$, combine these new functions with their SM counterparts, run all Wilson coefficients from the high energy scale $\mu \approx O(M_W)$ down to the lower energy scale $\mu = O(m_b)$ by using the QCD renormalization equations, find the effective Wilson coefficients C_i^{eff}, and finally calculate the branching ratios and CP-violating asymmetries after inclusion of NP contributions in the TC2 model.

In Sect. 4, we calculated the branching ratios for fifty-seven $B \to$ PP, PV decays in the SM and TC2 model, presented the numerical results in Tables 3–8 and displayed the $m_{\tilde{\pi}}$ and N_c^{eff} dependence of several interesting decay modes in Figs. 2–9. From these tables and figures, the following conclusions can be reached:

(1) The theoretical predictions in the TC2 model for all fifty-seven decay modes under study are well consistent with the experimental measurements and upper limits within one or two standard deviations.

(2) The theoretical uncertainties induced by varying k^2, η and $m_{\tilde{\pi}}$ are moderate within the range of $k^2 = m_b^2/2 \pm 2\,\text{GeV}^2$, $\eta = 0.34 \pm 0.08$ and $m_{\tilde{\pi}} = 200 \pm 100\,\text{GeV}$. The dependence on whether we use the BSW or LQSSR form factors are also weak. The N_c^{eff} dependences vary greatly for different decay modes.

(3) For most $B \to$ PP decay channels, the NP effects $\delta\mathcal{B}$ are large in size and insensitive to the variations of the effective number of colors N_c^{eff}. For many $B \to$ PV decays, however, the $\delta\mathcal{B}$ are sensitive to the variations of N_c^{eff}. It seems that the $B \to K\pi$ and $B \to K\eta'$ decay channels are good places to test the TC2 model.

(4) For most class-II, IV and V decay channels, such as $B \to \eta\eta^{(\prime)}$, $B \to K\pi$, $B \to K\eta'$, etc. the NP enhancements to the decay rates can be rather large, from 30% to 100% of the SM predictions. Enhancements this large will be measurable when enough B decay events are accumulated at B factories in the forthcoming years.

(5) For most decay modes, both new gluonic and electroweak penguins contribute effectively.

(6) For $B \to K\eta'$ decays, the new physics enhancements are significant, $\sim 50\%$, and insensitive to the variations of k^2, η, $m_{\tilde{\pi}}$ and N_c^{eff} within the considered parameter space.

Table 11. CP-violating asymmetries $\mathcal{A}_{CP}$ in $B \to \mathrm{PV}$ decays (in percent) with $b \to d$ transition in the SM using $\rho = 0.12$ and $N_c^{\mathrm{eff}} = 2, 3, \infty$ for $k^2 = m_b^2/2 \pm 2$ and $\eta = 0.34 \pm 0.8$. The first and second error of the ratios corresponds to $\delta k^2 = \pm 2$ and $\delta\eta = \pm 0.08$, respectively

Channel	Class	2	3	∞
$B^0/\bar{B}^0 \to \rho^+\pi^-/\rho^-\pi^+$	I-4	$3.2^{+1.2+22.3}_{-0.7-18}$	$3.2^{+1.2+22.3}_{-0.7-18}$	$3.4^{+1.3+22.3}_{-0.6-18}$
$B^0/\bar{B}^0 \to \rho^-\pi^+/\rho^+\pi^-$	I-4	$5.8^{+0.7+10.5}_{-1.8-8.8}$	$5.8^{+0.7+10.4}_{-1.9-8.9}$	$5.8^{+0.7+10.4}_{-1.8-8.9}$
$\overset{(-)}{B}{}^0 \to \rho^0\pi^0$	II-2	$-36.1^{+4.4+5.7}_{-1.1-4.8}$	$21.4^{+8.6+3.5}_{-5.1}$	$23.1^{+0.4+16.9}_{-1.8-16.4}$
$B^\pm \to \rho^0\pi^\pm$	III-1	$-4.1^{+2.9+0.8}_{-1.2-1.0}$	$-5.4^{+3.9+1.0}_{-1.8-1.6}$	$-10.7^{+10.2+2.0}_{-4.6-3.1}$
$B^\pm \to \rho^\pm\pi^0$	III-1	$2.7^{+0.7+0.4}_{-1.5-0.3}$	$3.0^{+0.8+0.5}_{-1.7-0.4}$	$3.6^{+0.9+0.5}_{-2.0-0.4}$
$\overset{(-)}{B}{}^0 \to \rho^0\eta$	II-2	$-49.4^{+10.7+2.3}_{-9.8-0.5}$	$24.9^{+7.7+4.2}_{-4.5-5.0}$	$63.8^{+2.3+1.8}_{-4.6-4.5}$
$\overset{(-)}{B}{}^0 \to \rho^0\eta'$	II-2	$8.8^{+0.5+2.7}_{+5.0-5.7}$	$-26.9^{+12.5+3.4}_{-39-2.0}$	$34.9^{+1.4+19.8}_{-6.5-17.4}$
$B^\pm \to \rho^\pm\eta$	III-1	$4.0^{+1.0+0.6}_{-2.3-0.5}$	$4.5^{+1.1+0.7}_{-2.5-0.6}$	$5.9^{+1.4+0.8}_{-3.2-0.7}$
$B^\pm \to \rho^\pm\eta'$	III-1	$3.9^{+1.1+0.9}_{-2.4-0.6}$	$4.5^{+1.2+1.0}_{-1.7-0.6}$	$5.9^{+1.6+1.1}_{-3.5-0.9}$
$\overset{(-)}{B}{}^0 \to \omega\pi^0$	II-2	$51.1^{+0.7+7.7}_{-0.9-10.7}$	$22.1^{+6.5+3.8}_{-3.7-4.5}$	$33.0^{+0.1+11.6}_{-0.8-14.4}$
$B^\pm \to \omega\pi^\pm$	III-1	$10.2^{+2.3+0.4}_{-4.9-0.7}$	$8.5^{+2.0+0.7}_{-4.4-0.9}$	$-2.1^{+1.6+0.4}_{-0.6-0.6}$
$\overset{(-)}{B}{}^0 \to \omega\eta$	II-2	$52.2^{+1.2+5.3}_{-3.3-11.0}$	$22.4^{+5.4+3.9}_{-3.0-4.6}$	$7.6^{+0.+17.4}_{-0.3-14.6}$
$\overset{(-)}{B}{}^0 \to \omega\eta'$	II-2	$32.3^{+0.9+17.0}_{-3.6-16.6}$	$39.9^{+20.4+5.1}_{-13.5-7.7}$	$21.3^{+0.1+15.9}_{-0.2-15.5}$
$\overset{(-)}{B}{}^0 \to \phi\pi^0$	V-2	$16.0^{+5.6+2.7}_{-4.1-3.2}$	$1.4^{+0.6+0.2}_{-0.4-0.3}$	$11.9^{+4.5+2.0}_{-2.5-2.4}$
$B^\pm \to \phi\pi^\pm$	V-1	$12.7^{+5.6+2.4}_{-3.0-2.6}$	$1.0^{+0.8+0.2}_{-0.3-0.1}$	$9.1^{+4.7+1.6}_{-2.4-1.9}$
$\overset{(-)}{B}{}^0 \to \phi\eta$	V-2	$16.0^{+5.6+2.7}_{-3.1-3.2}$	$1.4^{+0.6+0.2}_{-0.3-0.3}$	$11.9^{+4.5+2.0}_{-2.5-2.4}$
$\overset{(-)}{B}{}^0 \to \phi\eta'$	V-2	$16.0^{+5.6+2.7}_{-3.1-3.2}$	$1.4^{+0.6+0.2}_{-0.3-0.3}$	$11.9^{+4.5+2.0}_{-2.5-2.4}$
$B^\pm \to \bar{K}^{*0}K^\pm$	IV-1	$13.4^{+5.7+2.4}_{-3.0-2.8}$	$12.6^{+5.6+2.4}_{-2.9-2.6}$	$11.6^{+5.3+2.1}_{-2.8-2.1}$
$B^0/\bar{B}^0 \to \bar{K}^{*0}K_S^0/K^{*0}K_S^0$	IV-4	$13.8^{+5.8+2.5}_{-3.1-2.9}$	$13.2^{+5.7+2.4}_{-3.0-2.7}$	$12.3^{+5.5+2.2}_{-2.9-2.5}$
$B^\pm \to K^{*\pm}K_S^0$	V-1	$-7.9^{+5.0+1.2}_{-17-0.8}$	$-4.6^{+6.3+0.5}_{-30.3-0.2}$	$75.8^{+0.6+8.6}_{-12.2-12.3}$
$B^0/\bar{B}^0 \to K^{*0}K_S^0/\bar{K}^{*0}K_S^0$	IV-4	$-11.6^{+3.0+2.4}_{-5.8-2.1}$	$-10.1^{+2.6+1.9}_{-5.3-2.1}$	$-7.7^{+2.2+0.7}_{-4.3-1.5}$

Table 12. Same as in Table 11 but with the $b \to s$ transition

Channel	Class	2	3	∞
$\overset{(-)}{B}{}^0 \to \rho^0 K_S^0$	IV-1	$15.1^{+0.5+2.7}_{-1.1-3.1}$	$32.1 \pm 0.0^{+5.1}_{-6.2}$	$46.0^{+1.4+1.2}_{-0.6-3.6}$
$B^\pm \to \rho^0 K^\pm$	IV-1	$-17.9^{+9.5+3.0}_{-4.3-4.0}$	$-18.9^{+10.1+1.9}_{-4.9-1.6}$	$-9.7^{+5.1+1.8}_{-2.7-1.5}$
$\overset{(-)}{B}{}^0 \to \rho^- K^+$	I-1	$-11.7^{+7.2+1.0}_{-2.9-0.7}$	$-12.2^{+7.5+1.1}_{-3.0-0.9}$	$-13.0^{+8.0+1.4}_{-3.2-1.3}$
$B^\pm \to \rho^\pm K_S^0$	IV-1	$1.7^{+0.2+0.4}_{-0.1-0.4}$	$2.7^{+0.6+0.7}_{-0.3-0.6}$	$-2.3^{+2.1+0.5}_{-7.9-0.6}$
$B^\pm \to K^{*\pm}\eta$	IV-1	$-7.3^{+4.1-1.2}_{-2.1+1.5}$	$-7.3^{+4.1-1.3}_{-2.2+1.5}$	$-7.2^{+4.0+1.6}_{-2.1-1.4}$
$B^\pm \to K^{*\pm}\eta'$	III-1	$-29.4^{+16+3.6}_{-2.4-1.9}$	$-54.4^{+22.0-0.7}_{-0.8+2.4}$	$-83.0^{+47.4+2.4}_{-12.5-2.3}$
$\overset{(-)}{B}{}^0 \to K^{*0}\eta$	IV-1	$-1.8^{+0.6}_{-0.3} \pm 0.4$	$-1.0^{+0.1}_{-0.0} \pm 0.2$	$0.6^{+0.5+0.1}_{-1.0-0.2}$
$\overset{(-)}{B}{}^0 \to K^{*0}\eta'$	V-1	$-4.3^{+4.2}_{-0.3} \pm 1.0$	$4.4^{+8.1+1.0}_{-1.1-1.0}$	$15.3^{+7.5+3.2}_{-13-3.4}$
$\overset{(-)}{B}{}^0 \to K^{*+}\pi^-$	IV-1	$-13.8^{+8.0+2.6}_{-4.4-2.0}$	$-13.9^{+8.2+2.6}_{-4.5-2.0}$	$-14.0^{+8.2+1.6}_{-4.6-1.9}$
$\overset{(-)}{B}{}^0 \to K^{*0}\pi^0$	IV-1	$0.2^{+0.7+0.1}_{-1.2-0.0}$	$-1.7 \pm 0.0 \pm 0.4$	$-4.3^{+1.9+1.0}_{-1.0-0.9}$
$B^\pm \to K^{*\pm}\pi^0$	IV-1	$-11.3^{+6.5+2.2}_{-3.6-1.8}$	$-10.4^{+6.0+2.1}_{-3.2-1.7}$	$-8.7^{+4.9+1.9}_{-2.7-1.7}$
$B^\pm \to K^{*0}\pi^\pm$	IV-1	$-1.5 \pm 0.1^{+0.3}_{-0.4}$	$-1.5^{+0.1+0.4}_{-0.1-0.3}$	$-1.4^{+0.1+0.4}_{-0.0-0.3}$
$B^\pm \to \phi K^\pm$	V-1	$-1.5 \pm 0.1^{+0.3}_{-0.4}$	$-1.6 \pm 0.1 \pm 0.4$	$-2.5 \pm 0.1 \pm 0.6$
$\overset{(-)}{B}{}^0 \to \phi K_S^0$	V-2	$31.1 \pm 0.0^{+4.8}_{-5.9}$	$31.1 \pm 0.0^{+5.7}_{-5.9}$	$30.6 \pm 0.0^{+4.7}_{-5.8}$
$\overset{(-)}{B}{}^0 \to \omega K_S^0$	V-2	$23.5^{+1.4+3.8}_{-0.9+4.6}$	$31.4^{+1.2+4.1}_{-11.4-5.6}$	$24.2^{+1.1+4.0}_{-0.7-4.8}$
$B^\pm \to \omega K^\pm$	V-1	$-11.5^{+6.6+2.3}_{-3.7-2.0}$	$-17.8^{+10.3+2.7}_{-4.1-3.6}$	$0.2^{+0.4}_{-0.8} \pm 0.1$

Table 13. CP-violating asymmetries $\mathcal{A}_{CP}$ in $B \to$ PV decays (in percent) with $b \to d$ transitions in the TC2 model using $\rho = 0.12$, $\eta = 0.34$, $k^2 = m_b^2/2$, $m_{\tilde{\pi}} = 200\,\mathrm{GeV}$ and $N_c^{\mathrm{eff}} = 2, 3, \infty$

		TC2			$\delta\mathcal{A}_{CP}[\%]$		
Channel	Class	2	3	∞	2	3	∞
$B^0 \to \rho^+\pi^-$	I-4	6.5	6.1	5.4	104	88.1	62.5
$B^0 \to \rho^-\pi^+$	I-4	7.5	7.3	7.0	30.9	27.2	21.1
$\overset{(-)}{B^0} \to \rho^0\pi^0$	II-2	−36.7	20.8	24.7	1.7	−2.7	6.7
$B^\pm \to \rho^0\pi^\pm$	III-1	−4.3	−5.8	−11.0	7.3	7.0	3.1
$B^\pm \to \rho^\pm\pi^0$	III-1	2.9	3.2	3.9	6.6	6.5	6.4
$\overset{(-)}{B^0} \to \rho^0\eta$	II-2	−34.6	16.8	58.4	−29.9	−32.5	−8.4
$\overset{(-)}{B^0} \to \rho^0\eta'$	II-2	−1.5	−16.6	41.9	−117	−38.2	20.2
$B^\pm \to \rho^\pm\eta$	III-1	4.2	4.8	6.3	6.9	6.7	6.0
$B^\pm \to \rho^\pm\eta'$	III-1	4.2	4.8	6.3	7.7	7.5	7.1
$\overset{(-)}{B^0} \to \omega\pi^0$	II-2	48.8	21.8	41.0	−4.5	−1.3	24.3
$B^\pm \to \omega\pi^\pm$	III-1	10.6	8.9	−2.2	3.7	5.0	8.0
$\overset{(-)}{B^0} \to \omega\eta$	II-2	56.2	15.3	3.3	7.8	−31.5	−55.9
$\overset{(-)}{B^0} \to \omega\eta'$	II-2	41.6	66.0	23.1	28.6	65.6	8.1
$\overset{(-)}{B^0} \to \phi\pi^0$	V-2	16.8	0.7	9.3	5.4	−53.2	−22.1
$B^\pm \to \phi\pi^\pm$	V-1	13.6	0.4	6.9	7.4	−54.1	−23.8
$\overset{(-)}{B^0} \to \phi\eta$	V-2	16.8	0.7	9.3	5.4	−53.2	−22.1
$\overset{(-)}{B^0} \to \phi\eta'$	V-2	16.8	0.7	9.3	5.4	−53.2	−22.1
$B^\pm \to \bar{K}^{*0}K^\pm$	IV-1	10.6	9.9	8.9	−21.2	−21.8	−22.6
$\overset{(-)}{B^0} \to \bar{K}^{*0}K_S^0/K^{*0}K_S^0$	IV-4	11.1	10.5	9.7	−19.6	−20.3	−21.2
$B^\pm \to K^{*\pm}K_S^0$	V-1	−0.4	84.4	18.3	−94.5	−1951	−75.8
$\overset{(-)}{B^0} \to K^{*0}K_S^0/\bar{K}^{*0}K_S^0$	IV-4	−8.2	−6.8	−4.6	−29.0	−33.4	−40.4

The theoretical predictions for $\mathcal{B}(B \to K\eta')$ become now consistent with the CLEO data due to the inclusion of new physics effects in the TC2 model.

In Sect. 5, we calculated the CP-violating asymmetries $\mathcal{A}_{CP}$ for $B \to$ PP, PV decays in the SM and TC2 model, presented the numerical results in Tables 9–14 and displayed the $m_{\tilde{\pi}}$ and N_c^{eff} dependence of $\mathcal{A}_{CP}$ for the decays $B^\pm \to K^\pm\eta', \omega\pi^\pm$ in Figs. 10 and 11. In this paper, the possible effects of FSI on $\mathcal{A}_{CP}$ are neglected. From these tables and figures, the following conclusions can be drawn:

(1) Although there is no new weak phase introduced in the TC2 model, the CP-violating asymmetries $\mathcal{A}_{CP}$ can still be changed through interference between the ordinary tree/penguin amplitudes in the SM and the new strong and electroweak penguin amplitudes in the TC2 model.

(2) The CP-violating asymmetries depend weakly on whether we use the BSW or LQQSR form factors in calculations in both the SM and TC2 model.

(3) For most $B \to$ PP decays, the $\delta\mathcal{A}_{CP}$ are generally small or moderate in magnitude (10%–30%), and insensitive to the variation of $m_{\tilde{\pi}}$ and N_c^{eff}. But the four class-II decay modes $\overset{(-)}{B^0} \to \pi^0\pi^0, \eta^{(\prime)}\eta^{(\prime)}$ have strong N_c^{eff} dependences in both the SM and the TC2 model.

(4) For the $B \to$ PV decays, however, $\delta\mathcal{A}_{CP}$ can be rather large for many decay modes. For decay $B^0/\bar{B}^0 \to \rho^+\pi^-/\rho^-\pi^+$, the new physics correction is (60–100)% for $N_c^{\mathrm{eff}} = 2$–∞. For the decay $B^+ \to K^{*+}\bar{K}^0$ the correction can even reach a factor of 20 for $N_c^{\mathrm{eff}} = 2$. For most class-I, III and IV decays, the N_c^{eff} dependence and k^2 dependences of $\delta\mathcal{A}_{CP}$ are weak. For most class-V decays, however, the N_c^{eff} dependence of $\delta\mathcal{A}_{CP}$ is strong.

(5) For the measured five decay modes $B \to K\pi, K\eta', \omega\pi$, the new physics effects is only about −20% compared to the SM predictions. The theoretical predictions for these five decay modes in the SM and TC2 model are well consistent with the CLEO measurements.

Acknowledgements. The authors are very grateful to D.S. Du, K.T. Chao, C.S. Li, C.D. Lü, Y.D. Yang and M.Z. Yang for helpful discussions. Z.J. Xiao acknowledges the support by the National Natural Science Foundation of China under the Grant No.19575015 and 10075013, the Excellent Young Teachers Program of MOE, P.R. China and the Natural Science Foundation of Henan Province under the Grant No. 994050500.

Table 14. Same as in Table 13 but with $b \to s$ transitions

Channel	Class	TC2 2	TC2 3	TC2 ∞	$\delta\mathcal{A}_{CP}[\%]$ 2	$\delta\mathcal{A}_{CP}[\%]$ 3	$\delta\mathcal{A}_{CP}[\%]$ ∞
$\overset{(-)}{B^0} \to \rho^0 K_S^0$	IV-1	19.2	32.1	45.0	26.6	−0.09	−2.1
$B^\pm \to \rho^0 K^\pm$	IV-1	−8.9	−6.9	−2.8	−50.4	−63.3	−71.2
$\overset{(-)}{B^0} \to \rho^- K^+$	I-1	−18.2	−17.6	−16.4	55.2	44.1	26.0
$B^\pm \to \rho^\pm K_S^0$	IV-1	2.8	2.6	−2.1	65.1	−0.6	−9.5
$B^\pm \to K^{*\pm}\eta$	IV-1	−4.8	−5.1	−5.4	−33.6	−31.1	−25.2
$B^\pm \to K^{*\pm}\eta'$	III-1	−66.7	−90.3	−44.4	127	65.9	−46.5
$\overset{(-)}{B^0} \to K^{*0}\eta$	IV-1	−1.3	−0.8	0.3	−27.2	−20.9	−52.1
$\overset{(-)}{B^0} \to K^{*0}\eta'$	V-1	−24.2	−4.5	4.4	469	−203	−71.2
$\overset{(-)}{B^0} \to K^{*+}\pi^-$	IV-1	−9.5	−9.9	−10.6	−31.0	−28.5	−24.0
$\overset{(-)}{B^0} \to K^{*0}\pi^0$	IV-1	0.2	−1.6	−3.7	0.5	−8.0	−14.3
$B^\pm \to K^{*\pm}\pi^0$	IV-1	−6.6	−6.2	−5.5	−41.6	−39.8	−36.4
$B^\pm \to K^{*0}\pi^\pm$	IV-1	−1.2	−1.2	−1.1	−18.9	−19.5	−20.3
$B^\pm \to \phi K^\pm$	V-1	−1.3	−1.4	−2.2	−13.2	−13.2	−13.5
$\overset{(-)}{B^0} \to \phi K_S^0$	V-2	31.2	31.2	30.8	0.4	0.4	0.6
$\overset{(-)}{B^0} \to \omega K_S^0$	V-2	24.8	31.5	25.4	5.8	0.4	5.1
$B^\pm \to \omega K^\pm$	V-1	−8.5	−19.9	0.06	−25.9	11.6	−66.9

Table 15. CLEO measurements for $\mathcal{A}_{CP}$ in $B \to K\pi, K\eta', \omega\pi$ decays [22], and the corresponding theoretical predictions in the SM and TC2 model

Channel	$\mathcal{A}_{CP}^{\mathrm{exp}}$	90% CL region	$\mathcal{A}_{CP}^{\mathrm{SM}}$	$\mathcal{A}_{CP}^{\mathrm{TC2}}$
$B^\pm \to K^\pm\pi^0$	-0.29 ± 0.23	$[-0.67, 0.09]$	$[-0.001, 0.079]$	$[0.009, 0.058]$
$\overset{(-)}{B^0} \to K^\pm\pi^\mp$	-0.04 ± 0.16	$[-0.30, 0.22]$	$[0.015, 0.096]$	$[0.010, 0.080]$
$B^\pm \to K_S^0\pi^\pm$	$+0.18 \pm 0.24$	$[-0.22, 0.56]$	$[0.007, 0.017]$	$[0.006, 0.015]$
$B^\pm \to K^\pm\eta'$	-0.03 ± 0.12	$[-0.17, 0.23]$	$[0.003, 0.062]$	$[0.002, 0.047]$
$B^\pm \to \omega\pi^\pm$	-0.34 ± 0.25	$[-0.75, 0.07]$	$[-0.129, 0.007]$	$[-0.102, 0.031]$

Appendix A: Input parameters

In this appendix we present the relevant input parameters. We use the same set of input parameters for the quark masses, decay constants, Wolfenstein parameters and form factors as in [12].

(1) Input parameters of electroweak and strong coupling constant, gauge boson masses, B meson masses, light meson masses, $\cdots$, are as follows (all masses in units of GeV) [12,42]:

$$\begin{aligned}
\alpha_{\mathrm{em}} &= 1/128, \quad \alpha_{\mathrm{s}}(M_Z) = 0.118, \quad \sin^2\theta_W = 0.23, \\
G_{\mathrm{F}} &= 1.16639 \times 10^{-5}\ (\mathrm{GeV})^{-2}, \\
M_Z &= 91.187, \quad M_W = 80.41, \quad m_{B_d^0} = m_{B_u^\pm} = 5.279, \\
m_{\pi^\pm} &= 0.140, \quad m_{\pi^0} = 0.135, \quad m_\eta = 0.547, \\
m_{\eta'} &= 0.958, \quad m_\rho = 0.770, \quad m_\omega = 0.782, \\
m_\phi &= 1.019, \quad m_{K^\pm} = 0.494, \quad m_{K^0} = 0.498, \\
m_{K^{*\pm}} &= 0.892, \quad m_{K^{*0}} = 0.896, \\
\tau(B_u^\pm) &= 1.64\,\mathrm{ps}, \quad \tau(B_d^0) = 1.56\,\mathrm{ps}. \qquad \text{(A1)}
\end{aligned}$$

(2) For the elements of the CKM matrix, we use the Wolfenstein parameterization, and fix the parameters A, λ, ρ to their central values, $A = 0.81, \lambda = 0.2205, \rho = 0.12$ and vary η in the range of $\eta = 0.34 \pm 0.08$.

(3) We firstly treat the internal quark masses in the loops in connection with the function $G(x_i, z)$ as constituent masses,

$$\begin{aligned}
m_b &= 4.88\,\mathrm{GeV}, \quad m_c = 1.5\,\mathrm{GeV}, \quad m_s = 0.5\,\mathrm{GeV}, \\
m_u &= m_d = 0.2\,\mathrm{GeV}. \qquad \text{(A2)}
\end{aligned}$$

Secondly, we will use the current quark masses for m_i ($i = u, d, s, c, b$) which appear through the equation of motion when working out the hadronic matrix elements. For $\mu = 2.5\,\mathrm{GeV}$, one finds [12]

$$\begin{aligned}
m_b &= 4.88\,\mathrm{GeV}, \quad m_c = 1.5\,\mathrm{GeV}, \quad m_s = 0.122\,\mathrm{GeV}, \\
m_d &= 7.6\,\mathrm{MeV}, \quad m_u = 4.2\,\mathrm{MeV}. \qquad \text{(A3)}
\end{aligned}$$

For the mass of the heavy top quark we also use $m_t = \overline{m_t}(m_t) = 168\,\mathrm{GeV}$.

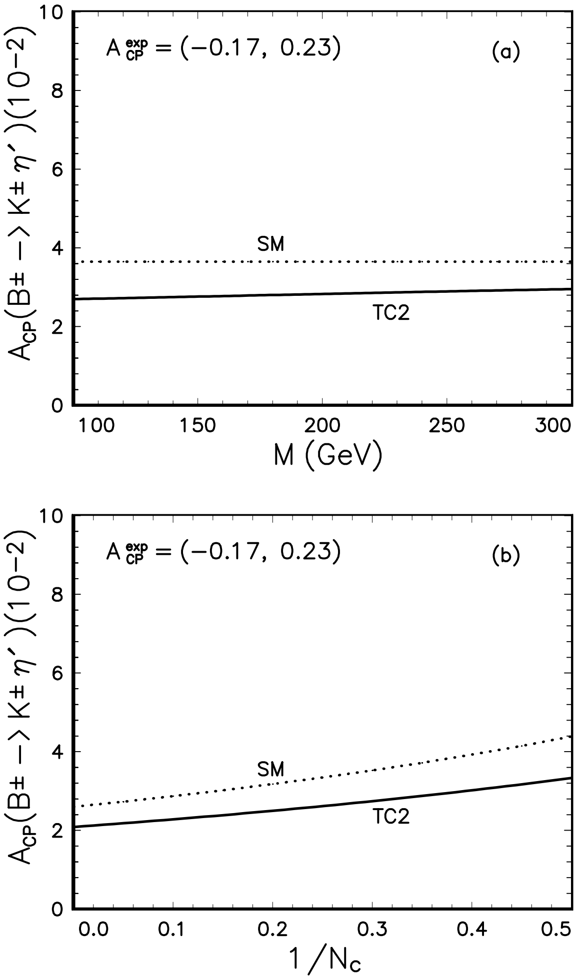

Fig. 10a,b. Plots of CP-violating asymmetries $\mathcal{A}_{CP}$ versus $m_{\tilde{\pi}}$ and $1/N_c^{\mathrm{eff}}$ for decay ($B^{\pm} \to K^{\pm}\eta'$). For **a** and **b** we set $N_c^{\mathrm{eff}} = 3$ and $m_{\tilde{\pi}} = 200\,\mathrm{GeV}$, respectively. The 90% C.L. allowed region from CLEO is $\mathcal{A}_{CP} = [-0.17, 0.23]$

(4) For the decay constants of the light mesons, the following values will be used in the numerical calculations (in units of MeV):

$$
\begin{aligned}
&f_\pi = 133, \quad f_K = 158, \quad f_{K^*} = 214, \\
&f_\rho = 210, \quad f_\omega = 195, \quad f_\phi = 233, \\
&f_\eta^u = f_\eta^d = 78, \quad f_{\eta'}^u = f_{\eta'}^d = 68, \quad f_\eta^c = -0.9, \\
&f_{\eta'}^c = -0.23, \quad f_\eta^s = -113, \quad f_{\eta'}^c = 141, \qquad \text{(A4)}
\end{aligned}
$$

where $f^u_{\eta^{(\prime)}}$ and $f^s_{\eta^{(\prime)}}$ have been defined in the two-angle-mixing formalism with $\theta_0 = -9.1^\circ$ and $\theta_8 = -22.2^\circ$ [61] For more details about the mixings between η and η', see [61,13].

Appendix B: Form factors

(1) The form factors at the zero momentum transfer in the Bauer, Stech and Wirbel (BSW) [15] model have been collected in Table 2 of [12]. For the convenience of the reader

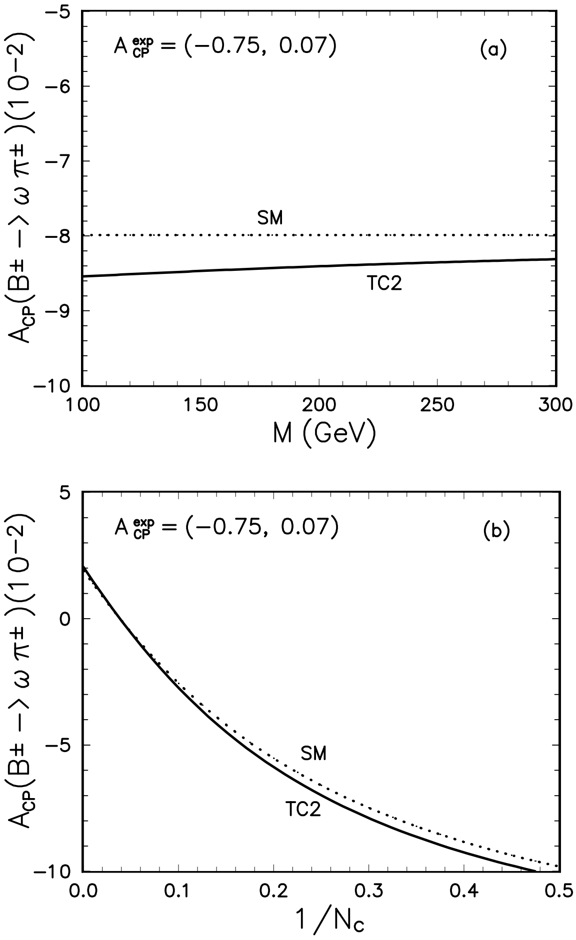

Fig. 11a,b. Same as Fig. 10 but for decay ($B^{\pm} \to \omega\pi^{\pm}$). The 90% C.L. allowed region from CLEO is $\mathcal{A}_{CP} = [-0.75, 0.07]$

we list them here:

$$
\begin{aligned}
&F_0^{B\pi}(0) = 0.33, \quad F_0^{BK}(0) = 0.38, \quad F_0^{B\eta}(0) = 0.145, \\
&F_0^{B\eta'}(0) = 0.135, \quad A_{0,1,2}^{B\rho}(0) = A_{0,1,2}^{B\omega}(0) = 0.28, \\
&A_0^{BK^*}(0) = 0.32, \quad A_{1,2}^{BK^*}(0) = 0.33, \\
&V^{B\rho}(0) = V^{B\omega}(0) = 0.33, \quad V^{BK^*}(0) = 0.37. \qquad \text{(B1)}
\end{aligned}
$$

(2) In the LQQSR approach, the form factors at zero momentum transfer used in our numerical calculations are [12]

$$
\begin{aligned}
&F_0^{B\pi}(0) = 0.36, \quad F_0^{BK}(0) = 0.41, \\
&F_0^{B\eta}(0) = 0.16, \quad F_0^{B\eta'}(0) = 0.145, \\
&\{A_0, A_1, A_2, V\}(B \to \rho) = \{0.30, 0.27, 0.26, 0.35\}, \\
&\{A_0, A_1, A_2, V\}(B \to K^*) = \{0.39, 0.35, 0.34, 0.48\}, \\
&\{A_0, A_1, A_2, V\}(B \to \omega) = \{0.30, 0.27, 0.26, 0.35\}. \qquad \text{(B2)}
\end{aligned}
$$

(3) The form factors $F_{0,1}(k^2)$, $A_{0,1,2}(k^2)$ and $V(k^2)$ were defined in [15] by

$$
F_0(k^2) = \frac{F_0(0)}{1 - k^2/m^2(0^+)}, \quad F_1(k^2) = \frac{F_1(0)}{1 - k^2/m^2(1^-)},
$$

$$A_0(k^2) = \frac{A_0(0)}{1 - k^2/m^2(0^-)}, \quad A_1(k^2) = \frac{A_1(0)}{1 - k^2/m^2(1^+)},$$
$$A_2(k^2) = \frac{A_2(0)}{1 - k^2/m^2(1^+)}, \quad V(k^2) = \frac{V(0)}{1 - k^2/m^2(1^-)}. \tag{B3}$$

(4) The pole masses used to evaluate the k^2 dependence of form factors are

$$\{m(0^-), m(1^-), m(1^+), m(0^+)\} = \{5.2789, 5.3248, 5.37, 5.73\} \tag{B4}$$

for the $\bar{u}b$ and $\bar{d}b$ currents. We have furthermore

$$\{m(0^-), m(1^-), m(1^+), m(0^+)\} = \{5.3693, 5.41, 5.82, 5.89\} \tag{B5}$$

for the $\bar{s}b$ currents.

References

1. P.F. Harrison, H.R. Quinn, editors, The BaBar physics book, SLAC-R-504, 1998
2. M.T. Cheng et al., Belle collaboration, KEK-Report 94-2; F. Takasaki, hep-ex/9912004; P. Eerola, Nucl. Instrum. Meth. A **446**, 384 (2000)
3. R. Fleischer, J. Matias, Phys. Rev. D **61**, 074004 (2000)
4. M. Misiak, S. Pokorski, J. Rosiek, in Heavy Flavor II, edited by A.J. Buras, M. Lindner (World Scientific, Singapore 1998), p. 795; S. Baek, P. Ko, Phys. Rev. Lett. **83**, 488 (1999); M. Ciuchini, E. Franco, G. Martinelli, A. Masiero, L. Silvestrini, Phys. Rev. Lett. **79**, 978 (1997)
5. D. Atwood, A. Soni, Phys. Rev. Lett. **81**, 3324 (1999); Phys. Rev. D **59**, 013007 (1999); D. Bowser-Chao, D. Chang, W.Y. Keung, Phys. Rev. Lett. **81**, 2028 (1999)
6. Y.L. Wu, L. Wolfenstein, Phys. Rev. Lett. **73**, 1762 (1994); L. Wolfenstein, Y.L. Wu, Phys. Rev. Lett. **73**, 2809 (1994); K. Huitu, D.X. Zhang, C.D. Lü, P. Singer, Phys. Rev. Lett. **81**, 4313 (1998); Y.F. Zhou, Y.L. Wu, Mod. Phys. Lett. A **15**, 185 (2000); C.S. Huang, W. Liao, Q.S. Yan, Phys. Rev. **59**, 011701 (1999); Y.L. Wu, Y.F. Zhou, Phys. Rev. D **61**, 096001 (2000)
7. T.M. Aliev, E.O. Iltan, Phys. Rev. D **58**, 095014 (1998); T.M. Aliev, G. Hiller, E.O. Iltan, Nucl. Phys. B **515**, 321 (1998); K. Kiers, A. Soni, G.H. Wu, Phys. Rev. D **59**, 096001 (1999); E.O. Iltan, Phys. Rev. D **60**, 034023 (1999)
8. C.D. Lü, Z.J. Xiao, Phys. Rev. D **53**, 2529 (1996); B. Balaji, Phys. Rev. D **53**, 1699 (1996); G.R. Lu, C.X. Yue, Y.G. Cao, Z.H. Xiong, Z.J. Xiao, Phys. Rev. D **54**, 5647 (1996); G.R. Lu, Z.H. Xiong, Y.G. Cao, Nucl. Phys. B **487**, 43 (1997); G.R. Lu, Z.J. Xiao, H.K. Guo, L.X. Lü, J. Phys. G **25**, L85 (1999)
9. Z.J. Xiao, C.S. Li, K.T. Chao, Phys. Lett. B **473**, 148 (2000); Z.J. Xiao, C.S. Li, K.T. Chao, Phys. Rev. D **62**, 094008 (2000)
10. H. Simma, D. Wyler, Phys. Lett. B **272**, 395 (1991); G. Kramer, W.F. Palmer, H. Simma, Nucl. Phys. B **428**, 77 (1994); Z. Phys. C **66**, 429 (1995); R. Fleischer, Phys. Lett. B **321**, 259 (1994); Z. Phys. C **62**, 81 (1994); G. Kramer, W.F. Palmer, Phys. Rev. D **52**, 6411 (1995); N.G. Deshpande, X.G. He, Phys. Lett. B **336**, 471 (1994); G. Kramer, W.F. Palmer, Y.L. Wu, Commun. Theor. Phys. **27**, 457 (1997); C.-W. Chiang, L. Wolfenstein, Phys. Rev. D **61**, 074031 (2000); T. Muta, A. Sugamoto, M.Z. Yang, Y.D. Yang, Phys. Rev. D **62**, 094020 (2000); M.Z. Yang, Y.D. Yang, Phys. Rev. D **62**, 114019 (2000)
11. D. Du, L. Guo, Z. Phys. C **75**, 9 (1997); J. Phys. G **23**, 525 (1997)
12. A. Ali, G. Kramer, C.D. Lü, Phys. Rev. D **58**, 094009 (1998)
13. A. Ali, C. Greub, Phys. Rev. D **57**, 2996 (1998); A. Ali, J. Chay, C. Greub, P. Ko, Phys. Lett. B **424**, 161 (1998)
14. Y.H. Chen, H.-Y. Cheng, B. Tseng, K.C. Yang, Phys. Rev. D **60**, 094014 (1999)
15. M. Bauer, B. Stech, Phys. Lett. B **152**, 380 (1985); M. Bauer, B. Stech, M. Wirbel, Z. Phys. C **29**, 637 (1985); ibid., C **34**, 103 (1987)
16. H.-Y. Cheng, Phys. Lett. B **335**, 428 (1994); B **395**, 345 (1997); H.-Y. Cheng, B. Tseng, Phy. Rev. D **58**, 094005 (1998)
17. A.J. Buras, L. Silvestrini, Nucl. Phys. B **548**, 293 (1999)
18. H.-Y. Cheng, Hsiang-nan Li, K.C. Yang, Phys. Rev. D **60**, 094005 (1999)
19. M. Bishai et al., CLEO Collaboration, CLEO CONF 99-13, hep-ex/9908018;S.J. Richichi et al., CLEO Collaboration, CLEO CONF 99-12, hep-ex/9908019;T.E. Coan et al., CLEO Collaboration, CLEO CONF 99-16, hep-ex/9908029;Y. Kwon et al., CLEO Collaboration, CLEO CONF 99-14, hep-ph/9908039
20. S.J. Richichi et al., CLEO Collaboration, Phys. Rev. Lett. **85**, 520 (2000)
21. D. Cronin-Hennessy et al., CLEO Collaboration, Phys. Rev. Lett. **85**, 515 (2000); C.P. Jessop et al., CLEO Collaboration, CLEO 99-19, hep-ex/0006008
22. S. Chen et al., CLEO Collaboration, Phys. Rev. Lett. **85**, 525 (2000); J. O'Neill, CLEO Collaboration, CLEO Talk 00-1; W. Sun, CLEO Collaboration, CLEO Talk 00-8; V. Frolov, CLEO Collaboration, CLEO Talk 00-22
23. For a summary of recent CLEO results: D. Jaffe, talk Presented at BNL Particle Physics Seminar, 20 April, 2000, CLEO-Talk 00-10
24. B. Aubert et al.,, BaBar Collaboration, paper submmitted to ICHEP'2000, Osaka, Japan, 27 July–2 August 2000, BaBar-Conf-00/14; J. Olsen, BaBar Collaboration, talk given at DPF'2000, Columbus Ohino, USA, August 2000, BaBar-talk-00/27
25. A. Abashian et al., Belle Collaboration, talks given at ICHEP'2000, Osaka, Japan, 27 July–2 August 2000, Conf-0005, Conf-0006, Conf-0007
26. A. Ali, G. Kramer, C.D. Lü, Phys. Rev. D **59**, 014005 (1999)
27. G. Buchalla, A.J. Buras, M.E. Lautenbacher, Rev. Mod. Phys. **68**, 1125 (1996)
28. A.J. Buras, R. Fleischer, in Heavy Flavor II, edited by A.J. Buras, M. Lindner (World Scientific, Singapore 1998), p. 65; A.J. Buras, in Probing the standard model of particle interactions, edited by F. David, R. Gupta (Elsevier Science, 1998), hep-ph/9806471
29. H.J. Lipkin, hep-ph/0009241
30. C.T. Hill, Phys. Lett. B **345**, 483 (1995)
31. For more details about TC2 models and experimental constraints, see K. Lane, presented at the 28th International Conference on High Energy Physics, Warsaw (July 1996), ICHEP 96:367–378

32. S. Weinberg, Phys. Rev. D **13**, 974 (1976); D **19**, 1277 (1979); L. Susskind, ibid., D **20**, 2619 (1979)
33. E. Farhi, L. Susskind, Phys. Rev. D **20**, 3404 (1979)
34. G. Buchalla, G. Burdman, C.T. Hill, D. Kominis, Phys. Rev. D **53**, 5185 (1996)
35. D. Kominis, Phys. Lett. B **358**, 312 (1995)
36. G. Burdman, D. Kominis, Phys. Lett. B **403**, 101 (1997); G. Burdman, Phys. Lett. B **409**, 443 (1997)
37. E. Eichten, I. Hinchliffe, K. Lane, C. Quigg, Rev. Mod. Phys. **56**, 579 (1984); Phys. Rev. D **34**, 1547 (1986); E. Eichten, K. Lane, Phys. Lett. B **327**, 129 (1994)
38. Z.J. Xiao, L.X. Lü, H.K. Guo, G.R. Lu, Eur. Phys. J. C **7**, 487 (1999)
39. J. Ellis, M.K. Gaillard, D.V. Nanopoulos, P. Sikivie, Nucl. Phys. B **182**, 505 (1981)
40. K. Lane, Phys. Rev. D **54**, 2204 (1996)
41. Z.J. Xiao, C.S. Li, K.T. Chao, Eur. Phys. J. C **10**, 51 (1999)
42. Particle Data Group, C. Caso et al., Eur. Phys. J. C **3**, 1 (1998)
43. T. Inami, C.S. Lim, Prog. Theor. Phys. **65**, 297 (1981)
44. R. Fleischer, Z. Phys. C **58**, 483 (1993)
45. H.-Y. Cheng, K.C. Yang, Phys. Rev. D **62**, 054029 (2000)
46. S.A. Abel, W.N. Cottingham, I.B. Whittingham, Phys. Rev. D **58**, 073006 (1998)
47. M. Bander, G. Silverman, A. Soni, Phys. Rev. Lett. **43**, 242 (1979)
48. J.M. Gérard, W.S. Hou, Phys. Rev. D **43**, 2909 (1991)
49. N.G. Deshpande, J. Trampetic, Phys. Rev. D **41**, 2926 (1990)
50. J. Bijnens, F. Hoogeveen, Phys. Lett. B **283**, 434 (1992)
51. H.Y. Cheng, invited talk at 3rd International Conference on B Physics and CP Violation (BCONF99), Taipei, Taiwan, 3–7 December 1999; hep-ph/9912372
52. B.H. Behrens et al., CLEO Collaboration, Phys. Rev. Lett. **80**, 3710 (1998)
53. A. Gritsan, talk presented at UCSB, UCSD, LBNL, SLAC, CU-Boulder, March–May 2000, CLEO TALK 00-20
54. H.J. Lipkin, Phys. Lett. B **433**, 117 (1998)
55. G.C. Branco, L. Lavoura, J.P. Silva, CP violation (Oxford University Press, 1999)
56. R. Waldi, Fortschr. Phys. **47**, 707 (1999)
57. F. Abe et al., CDF Collaboration, Phys. Rev. Lett. **81**, 5513 (1998)
58. Y.H. Chen, H.Y. Cheng, B. Tseng, Phys. Rev. D **59**, 074003 (1998)
59. X.G. He, W.S. Hou, K.C. Yang, Phys. Rev. Lett. **81**, 5738 (1998); J. Charles, Phys. Rev. D **59**, 054007 (1999); M. Neubert, JHEP, **9902**, 014 (1999); N.G. Deshpande, X.G. He, W.S. Hou, S. Pakasa, Phys. Rev. Lett. **82**, 2240 (1999)
60. Z.J. Xiao et al., in praperation
61. T. Feldmann, P. Kroll, Eur. Phys. J. C **5**, 327 (1998)